Characterization and quality assurance of micro-twisted pair cables and signal transmission studies for the Mu3e vertex pixel detector

Master's Thesis

Author:
Nicola Gubler
gublerni@student.ethz.ch

Supervisor:
Supervisor UZH: Prof. Dr. Olaf Steinkamp
Supervisor ETH: Prof. Dr. Rainer Wallny

January 9, 2024

Abstract

The Mu3e Experiment at the Paul Scherrer Institute (PSI) plans to find a lepton number violation in the decay of the muon into three electrons with a detector.
The detector needs to be constructed with a significantly low material budget to reduce the effects of multiple scattering.
Two of the elements specially designed for this experiment are the micro-twisted pair cable, which provides data connections between the detector and the DAQ system, and a special sensor chip called MuPix11 for the pixel detectors.
On the one hand, this thesis shows that the planned micro-twisted pair cables for the experiment offer the possibility to transmit data, but for that, a pre-emphasis is necessary. In addition, the impedance, insertion loss, and crosstalk were measured for the cables and a QC test was developed using these measurements to test the functionality of further cables.
On the other hand, the thesis also shows a method to optimize the data transfer from the ladders, made of MuPix11, to the Data Acquisition System (DAQ) system. Furthermore, some optimized DAC values are shown for an available ladder.

Contents

Chapter 1

Introduction

1.1 Motivation

The Standard Model of Particle Physics essentially summarizes particle physics as it stands today. The model describes all known elementary particles and their interactions, which are described by Quantum Chromodynamics (QCD), the weak interaction, and the electromagnetic interaction, unified by the electroweak interaction. The only interaction not considered in the model is gravitation.
The model has already been used to experimentally test many predictions. However, some questions are still open and need to be clarified in further experiments.

One of these planned experiments is the Mu3e experiment. This is to be carried out at the PSI [1] at the proton source. The Mu3e experiment will search for the charged lepton flavor violation $\mu^+ \rightarrow e^+e^-e^+$. Such a decay would indicate that physics beyond the standard model would exist.
A high sensitivity is necessary to measure the decay of certain particles, which requires special measuring instruments. This experiment needs a low material budget because the particles have low energy. This means that all elements used in the tracking system must meet this criterion. To meet these requirements, HV-MAPS are used as sensors, and micro-twisted pair cables are used as data cables of the vertex and SciFi sensors. Both the sensor and the data cable were designed specifically for this experiment.

The Mu3e experiment aims to achieve a data rate of $1.25\,\mathrm{Gbits}^{-1}$ at the vertex detector, which requires stable communication among all elements. To achieve this, it is necessary first to develop a quality control test that every element, especially the micro-twisted pair cables, will later need to pass.
On the other hand, examining the setting Digital to Analog Converter (DAC) values for the HV-MAPS to optimize transmission quality is essential.

The following text examines two aspects of the Mu3e experiment.
In Chapter 3, a characterization of the micro-twisted pair cable used in some of the detectors is presented. The cable's impedance, insertion loss, crosstalk, eye diagrams, and bit error rate are measured and found sufficient for the experiment. However, some differences were observed compared to a similar cable used in another experiment.
Chapter 4 provides an initial characterization of the ladder consisting of MuPix11 sensors used in the Mu3e experiment. The chapter describes the optimal communication settings for the ladder, as determined by experimental measurements.

1.2 The Standard Model

The Standard Model of Particle Physics is a theory that summarizes all particles and their interactions. All the particles are summarized in Figure 1.1.
Particles interact with each other through the exchange of Gauge Bosons, which have a spin of 1. The fundamental forces of nature are carried by different types of bosons. For instance, the electromagnetic force is carried by photons, the strong force by gluons, and the weak force by Z and W bosons.
The fermions, with Spin $\frac{1}{2}$, are responsible for covering matter. The fermions can be divided into leptons and quarks, and both of them can furthermore be divided into 3 generations. All fermions have an associated antiparticle with the same mass and spin but an opposite charge. The quarks carry a color charge, allowing them to interact through the strong force.
The Higgs Boson is the final particle in the standard model and is responsible for coupling with particles through the Higgs mechanism to give them mass[2].

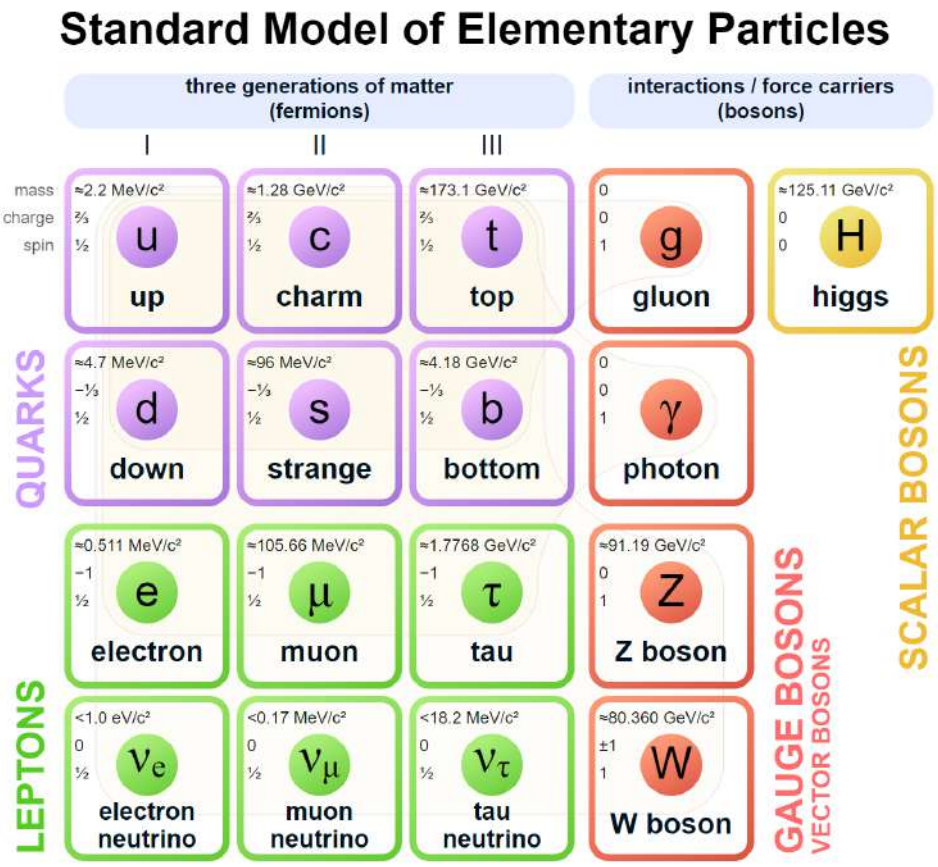

Figure 1.1: Standard Model of Particle Physics[3].

Feynman diagrams are used to visualize interactions of particles from the standard model.

In the standard model, some conservation variables must be taken into account in all interactions, which corresponds to Feynman diagrams vertices.
Some experiments have already shown that oscillations between different neutrinos occur and that this leads to violations of the lepton number[4].
This motivates the search for further lepton number violations, for example, in the muons.

1.3 Muon Decay

Muons are unstable particles that decay via weak interaction. The dominant decay, which preserves all conservation laws, is the Michel decay $\mu^+ \to \bar{\nu_\mu} e^+ \nu_e$ and $\mu^- \to \nu_\mu e^- \bar{\nu_e}$. This has a branching ratio of almost 1[6].
However, other decay is possible in the Standard Model with neutrino oscillations, but the theoretical branching ratio of $< 10^{-50}$ [7] indicates that this is very unlikely.
With such a small branching ratio, even a single observation of decay from $\mu^+ \to e^+ e^- e^+$ or $\mu^- \to e^- e^+ e^-$ would constitute a lepton number violation[8].
Furthermore, in the Mu3e experiment, which searches for decays from $\mu^+ \to e^+ e^- e^+$, it should be noted that the next leading order process of the Michel decay $\mu^+ \to e^+ e^- e^+ \bar{\nu_\mu} \nu_e$ might produce background, which must be taken into account. This is basically a Michel decay, in which the positron emits a photon, which in turn decays into an electron-positron pair. The branching ratio is $6.0(5) \times 10^{-8}$.

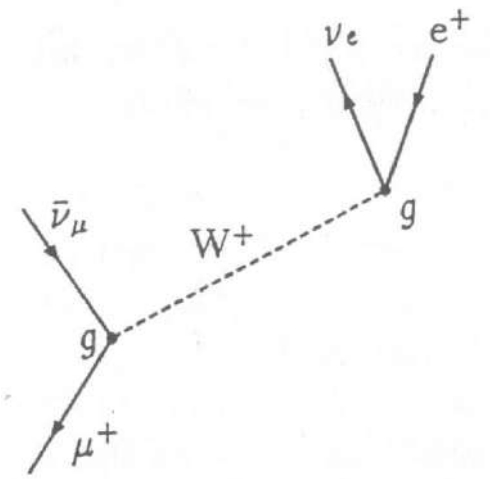

Figure 1.2: Michel decay[5].

In addition to the oscillations of neutrinos, as shown in Figure 1.3a, there are also theories that go beyond the standard model. With these theories, a significantly higher branching ratio would be expected. One of these theories is supersymmetry, which introduces new particles that would allow further lepton number violating decays. Such a lepton number violating decay is shown in Figure 1.3b.

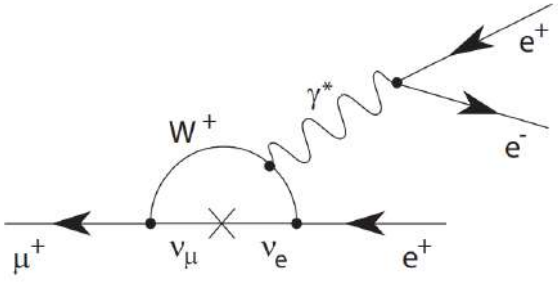

(a) μ^+ decay via Neutrino Oscillation.

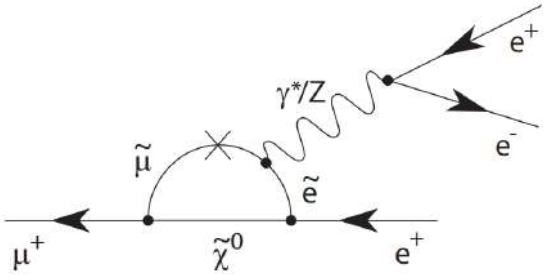

(b) μ^+ decay via supersymmetric particles.

Figure 1.3: Feynmann diagrams for $\mu^+ \to e^+ e^- e^+$ decays[8].

Chapter 2

Mu3e Experiment

The Mu3e experiment will be performed at the PSI in Villigen, Switzerland. The experiment aims to find the flavor-violating decay $\mu^+ \to e^+e^-e^+$. A muon beam is used for this measurement, which is stopped at a target.
The sensitivity of the branching ratio to be achieved is 2×10^{-15} for phase 1 of the experiment and 1×10^{-16} for phase 2 of the experiment[8].
To achieve such a high sensitivity, a muon source with a rate $\geq 2 \times 10^9$ Hz is required. The High-Intensity Muon Beamline (HiMB), which is expected to deliver $1 \times 10^{10}\,\mu s^{-1}$, is still in the design phase and therefore not yet installed. Until this beamline is operational, Run 1 of the experiment will be performed on the current $\pi E5$ beamline at PSI with a muon rate of $1 \times 10^8\,\mu s^{-1}$. For phase 2 of the experiment, it is then planned to use the HiMB.

Figure 2.1: The Mu3e logo[1].

The SINDRUM experiment from 1983 to 1986 determined the best limit of the $\mu^+ \to e^+e^-e^+$ decay to date. At that time, the branching ratio was determined to be 1×10^{-12} with a confidence level of 90% [9].

Figure 2.2 shows an overview of the planed systems at PSI, with the HiMB colored in green.

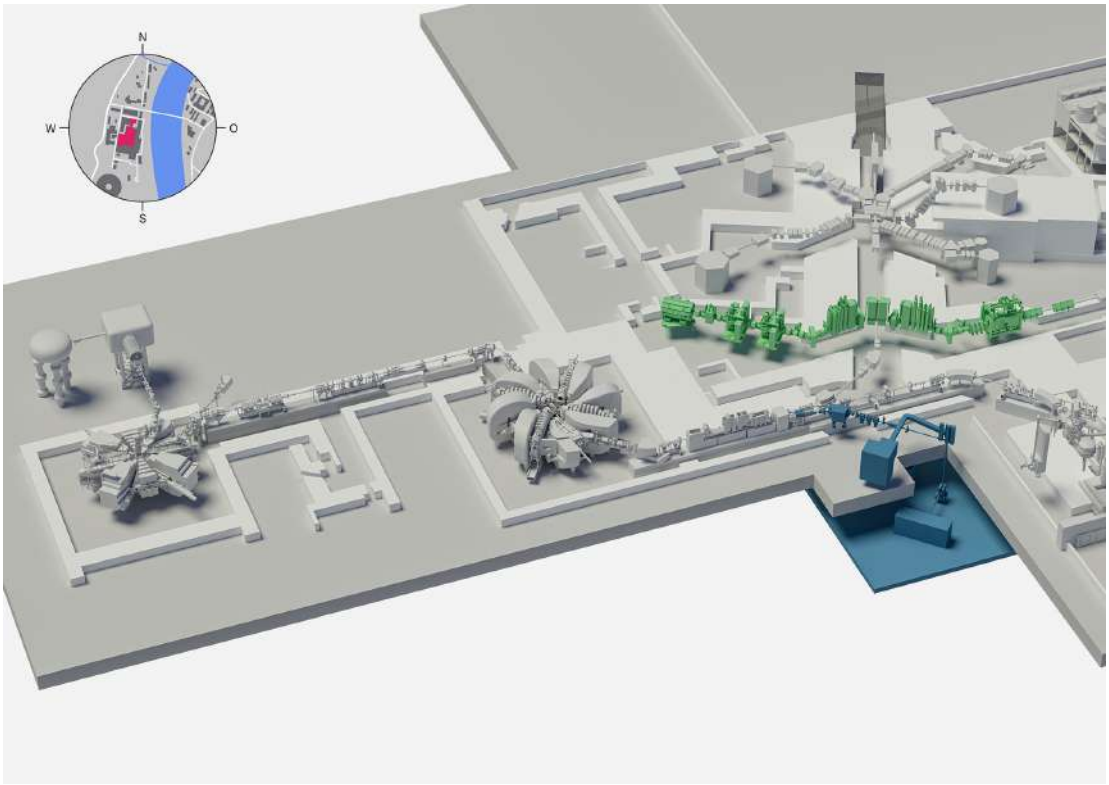

Figure 2.2: Overview of the equipment in the west wing of PSI. The upgraded HiMB is highlighted in green. A new production facility for more and better pharmaceuticals is highlighted in dark blue.[10].

2.1 Signal and Background

The total energy of the muon in the rest system corresponds to $E_0 = m_\mu c^2 \approx 106\,\mathrm{MeV}$. Due to the conservation of energy in the rest system, when $\mu^+ \to e^+e^-e^+$ decays, none of the electrons can exceed more than half the rest energy of the muon. Furthermore, it must also be noted that all three electrons originate from the same spacetime point.
These two constraints can be used to suppress background events. The background events can be divided into the following two categories:
Accidental background events occur when two different Michel decays combined appear as an $\mu^+ \to e^+e^-e^+$ decay due to the high muon rate and the limited detector resolution. They scale with the beam intensity[8].
Irreducible background in the Mu3e experiment consists of decays such as the radioactive decay with the internal conversion $\mu^+ \to e^+e^-e^+\nu\nu$. They depend strongly on the resolution and the granularity of the detector[8].

2.2 Multiple Scattering

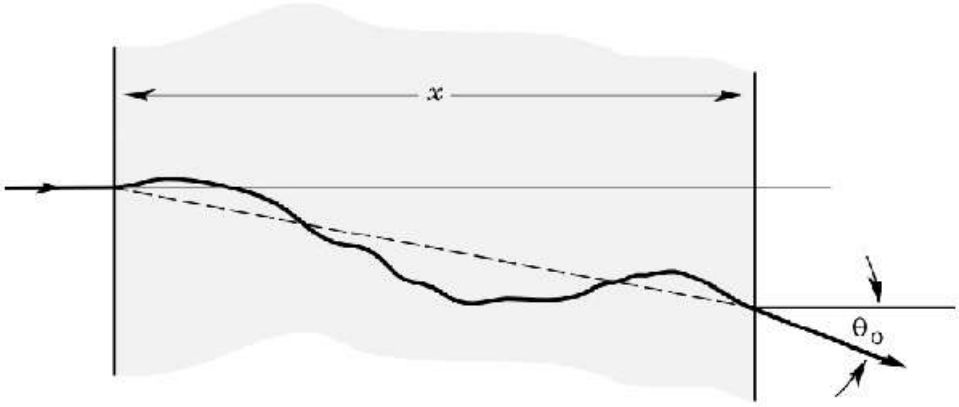

Figure 2.3: Particle passing through matter and gets deflected by multiple scattering[11].

Figure 2.3 shows the path of a particle through a material. It can be seen that deflections occur. This is due to the fact that particles traveling through the material are deflected by the Coulomb field. The Highland equation [12] describes the root mean square of this deflection.

$$\theta_0 = \frac{13.6}{\beta cp} z \sqrt{x/X_0} \left[1 + 0.038 \ln \left(x/X_0\right)\right]$$

In this equation, z corresponds to the penetration depth, p to the momentum of the particle, (βc) to the velocity of the particle, x to the thickness of the material through which the particle passes, and X_0 to the radiation length of the material.
Changing the trajectory of the particles by multiple scattering limits the available resolution of the detector. The low energy of the leptons in the Mu3e experiment is, therefore, a major problem.
To prevent multiple scattering, the traveled distance x in the material must be kept as small as possible and therefore, parts of the detector (except the last detector) must be as thin as possible.

2.3 Mu3e detector

The Mu3e experiment's phase 1 detector will consist of three parts. A central station and an upstream and downstream deflection station. Which were all arranged in a cylinder shape.
To observe the rare $\mu^+ \to e^+e^-e^+$ decay, an excellent resolution of the detector is necessary. For good momentum and vertex resolution, a silicon pixel tracker with low material usage is located in the central and the outer stations. Fiber detectors are used in the central and outer stations to obtain good time resolution[8].
The muons from the accelerator hit a hollow double-cone-shaped Mylar stopping target in the central station of the detector, in which the decay products are distributed in the longitudinal direction[13].

Pixel tracker layers 1 and 2 are located directly around the stopping target in the central station. Pixel tracker layers 3 and 4 are located further out. The inner two layers together in the central station are called the vertex detector. This detector enables a precise reconstruction of the paths of charged particles that are created during the collisions. The vertex detector is used to record the position of particle collisions with high accuracy and thus provide important information about the resulting particles and their interactions[13].
A fiber detector called Scintilating Fibre (SciFi) detector is placed directly in the third layer in the central station to better distinguish between the track and the timestamp. The time resolution of this detector is 250 ps[14].

The entire detector is in a 1 Tesla solenoidal solid magnetic field. Thanks to this magnetic field, the momentum of the decay electrons can be measured. Through this magnet, the electrons move along a spiral path. This causes them to hit either the tracker of the central station or one of the two upstream or downstream deflection stations again[13].

The two upstream and downstream stations consist of two more layer pixel sensors arranged in the same radius as layers 3 and 4. Inside the inner layer is another fiber detector called the SciTile detector for measuring the timestamp. Since this is the last detector in which the electrons are measured, it can have a much larger diameter and, therefore, has with 23.3 ps a better time resolution than the SciFi detector of the central station[13].
Figure 2.4 shows a cross-section of the planned phase 1 Mu3e tracker.

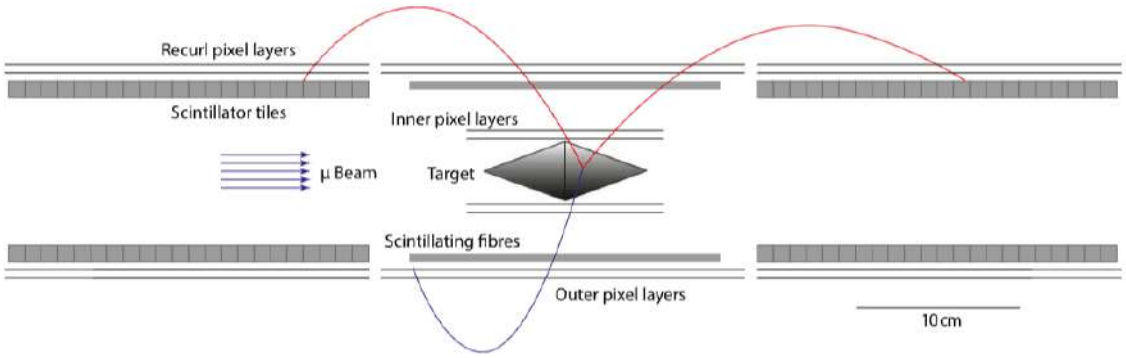

Figure 2.4: Schematic view of the phase 1 Mu3e experiment, with a cut along the beam axis.[13]

2.4 Pixel Detector

The pixel detector in the Mu3e experiment consists of 4 layers, as shown in Figure 2.4. All these layers consist of modules built of ladders, which in turn consist of HV-MAPS sensors, which are called MuPix sensors in the context of the Mu3e experiment. To dissipate the heat, the detectors are cooled with the help of helium.
The outer two pixel layers are equipped with additional fiber Time of flight (ToF) detectors for better time measurement.

2.4.1 High-Voltage Monolithic active pixel sensor (HV-MAPS)

The HV-MAPS technology is a pixel sensor technology, which was developed by Ivan Peric[15]. These sensors are manufactured using a Commercial Metal-Oxide-Semiconductor (CMOS) process and are qualified for high voltages up to 120 V.
HV-MAPS are designed in a way that both the sensing and readout electronics are integrated into a single chip. In contrast, hybrid pixel detectors consist of a separate sensor layer, usually a silicon detector, and a readout electronics chip that is then bump-bonded together[16].
HV-MAPS are commonly used for various reasons, as discussed in [17]. They are particularly cost-effective because they do not require bump-bonding and have commercial applications [18].
Due to the low material budget, a reduction in thickness is necessary to prevent multiple scattering, which is only possible thanks to the HV-MAPS technology, which does not require bump bonding. Additionally, HV-MAPS provides good time resolution, which is crucial for decay peak reconstruction[18].

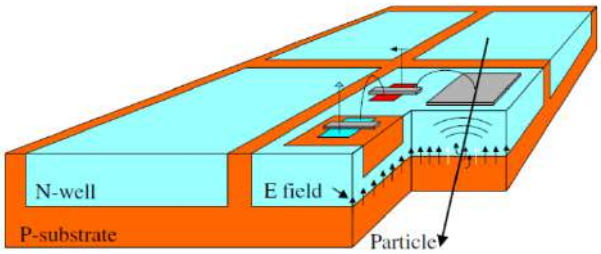

Figure 2.5: Working principle of a HV-MAPS Detector[19].

2.4.2 MuPix11 Sensor

The sensor developed for the tracking system of the Mu3e experiment is the MuPix11.
In phase 1 of the experiment, the MuPix 11 is planned to be used in the central and outer layers. In order to meet the very low material budget required for the experiment, HV-MAPS technology will be used as it can be thinned to low thicknesses.
MuPix11 are produced in thicknesses of 50 µm for the vertex detector and 70 µm for the outer layers.
Figure 2.6 shows the structure of a MuPix11 sensor.
The active area of the sensor is divided into three sub-matrices, each of which is read out separately.
The electronics are located in the periphery. This is where the rapidly changing digital signals are separated from the analog signals in order to minimize crosstalk.
In addition, the periphery contains some connection pads that can be used for testing and operation[20].

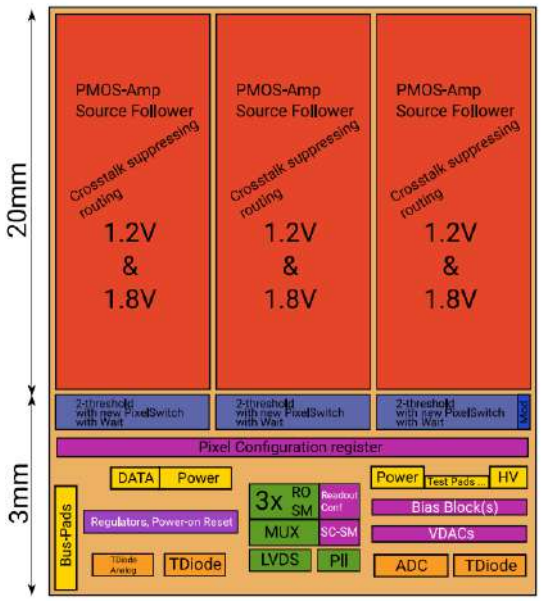

Figure 2.6: MuPix 11 block diagram (not to scale)[13].

Chip Design

This section explains how a Mupix11 sensor works. The signal is measured in the pixel and then transmitted to the periphery.
Figure 2.8 shows a schematic representation of the readout concept.

Pixels: MuPix11 consists of 64,000 pixels, with each pixel having a size of 80 µm times 80 µm.
Figure 2.7 shows the structure of a single pixel.
When a charged particle passes through the depleted zone of a pixel, it interacts with the sensing material and creates electron-hole pairs. The depleted zone is a region that has been intentionally depleted of free charge carriers (electrons and holes) by applying a bias voltage across the pixel electrodes. This creates an electric field in the depleted zone, which enables the separation and collection of the charge carriers created by the particle interaction. The electron-hole pairs created by the charged particle are separated by the electric field and drift towards the pixel electrode, generating a current that is proportional to the number of charge carriers created[21]. The pulse is then separately in each pixel amplified by a Charge sensitive amplifier (CSA). After this amplification, the pulses are

getting transferred into the peripheries[19].

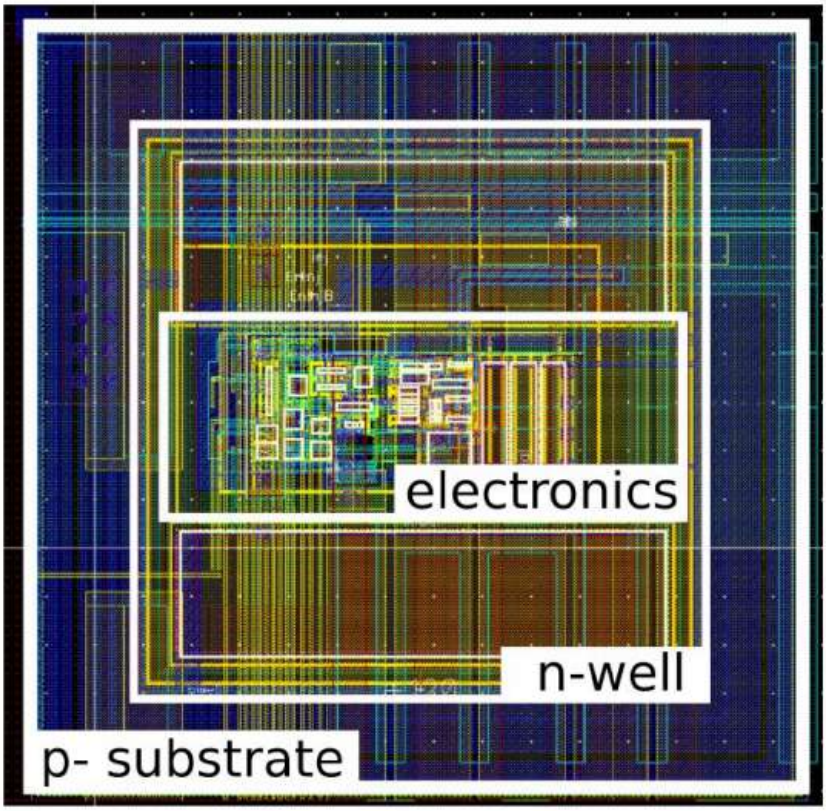

Figure 2.7: A Pixel of a MuPix11.[22]

Peripherie: The pulses from the pixel are then sent to the peripheries. There, two comparators are used to convert the analog signal into a digital signal. The signals are compared to see if they are higher than the respective threshold values. This is the value ThLow for one comparator, and for the other, ThHigh. If this is the case, the comparator calculates the Time over Threshold (ToT), i.e. the time in which the signal exceeds the respective threshold value. These two values can also be adjusted separately for each pixel. If the ToT is recorded by a comparator, the time stamp is also registered[19].

State machine: After digitizing the signal in the periphery, the data for each submatrix is collected separately in the state machine. This encodes the data in an 8b/10b process and serializes it. The data is then sent at a $1.25\,\mathrm{Gbits}^{-1}$ transmission speed[19].

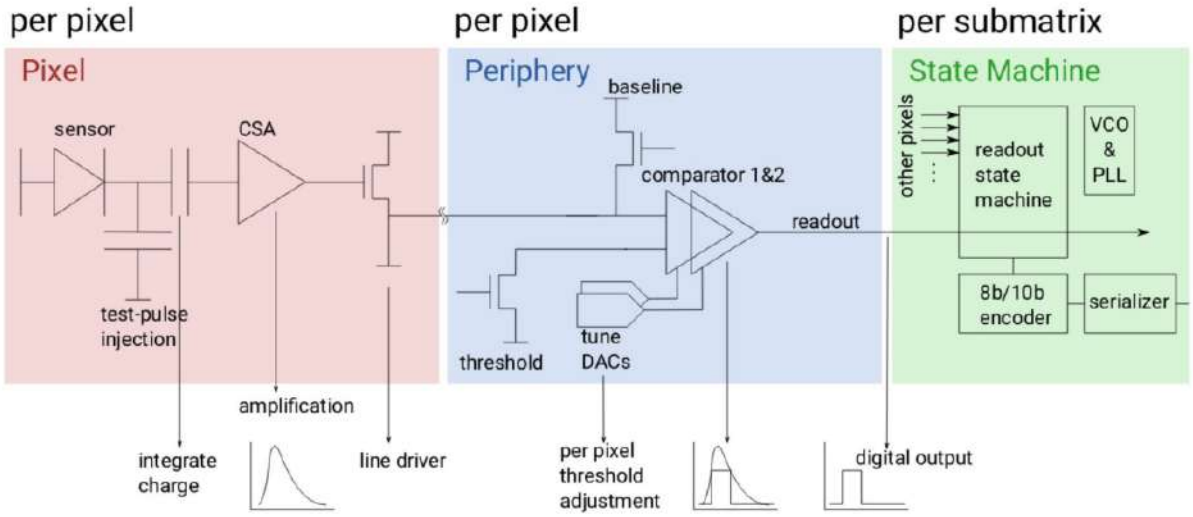

Figure 2.8: Readout concept of the MuPix11.[22]

Digital to Analog Converter (DAC)

Many values of the MuPix sensor, such as the height of the threshold but also, for example, the amplitude for signal transmission via the micro-twisted pair cables, can be controlled via so-called DACs.
These can be addressed on the software side using binary values, which in turn results in an analog signal for the component that controls the desired electrical value.
This is, therefore, a very important tool for optimizing things on the sensor, such as signal transmission quality.
However, the accuracy of setting the DAC values depends on the accuracy of the possible DAC values.

The Tuning/Trimming Digital to Analog Converter (TDAC) is the DAC used on the Mupix11 sensor and consists of 7 bits, whereby the first bit is responsible for masking, which means that the first bit indicates whether the sensor is digitally activated or deactivated. Therefore, the other 6 bits can transmit up to $2^6 = 64$ different values.

2.4.3 Sensor Mounting

These sensors are then mounted on a line on a carrier structure called High-Density Interconnect (HDI), which is made out of thin kapton-aluminium foil to meet the material budget. This HDI board serves as a supply and support structure for the chips. The chips are supplied with low-voltage and high-voltage current via the HDI and via the HDI control signals and data are transmitted to the ladder.
The detectors are bounded to the HDI via Single-point Tape- Automated Bonding (SpTAB),

which is permanent. This means that the sensors have to be carefully tested before mounting.

The vertex ladders (layers 1 and 2) contain 6 chips per ladder (18 ladders in total), the other layers and the layers in the outer stations consist of ladders with 17 or 18 chips each (52 ladders in total)[23]. The ladders are assembled into modules of 8 in the inner layer and 10 in the outer layer before final assembly. These modules are then assembled into the final layers. For layer 1, this can be seen in Figure 2.5.

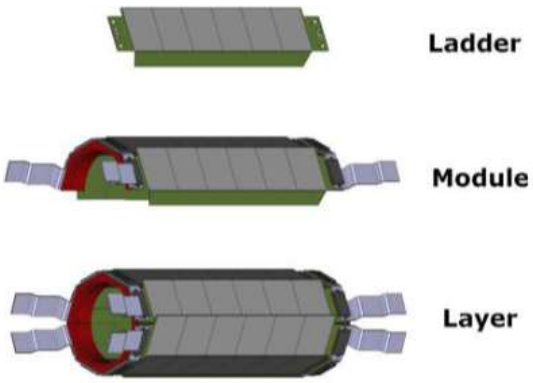

Figure 2.9: Tracker Layer 1 assembly built up from ladders over modules to layers.[13]

2.5 The Scintilating Fibre (SciFi) Detector

A cylindrical ToF detector called SciFi detector is planned inside the outer Pixel layers. This detector consists of 250 mm thin, double-sheathed scintillating fibers and a readout system. This ToF detector is there to precisely measure the arrival time of the particles with a time resolution of 250 ps, in order to compare the hits with the hits in the neighboring silicon detector.
With this detector, it is also possible to find the direction of the particle flight, from which the charge can be determined[13],[8].
A readout system is attached to the end of the scintillating fibers. The silicon photomultipliers, which are placed at the end of the fibers, detect the scintillating light generated in the fibers. A Muon Timing Resolver including Gigabit-link (MuTRiG) connected to the photomultiplier via flex prints serves as a readout device[24].

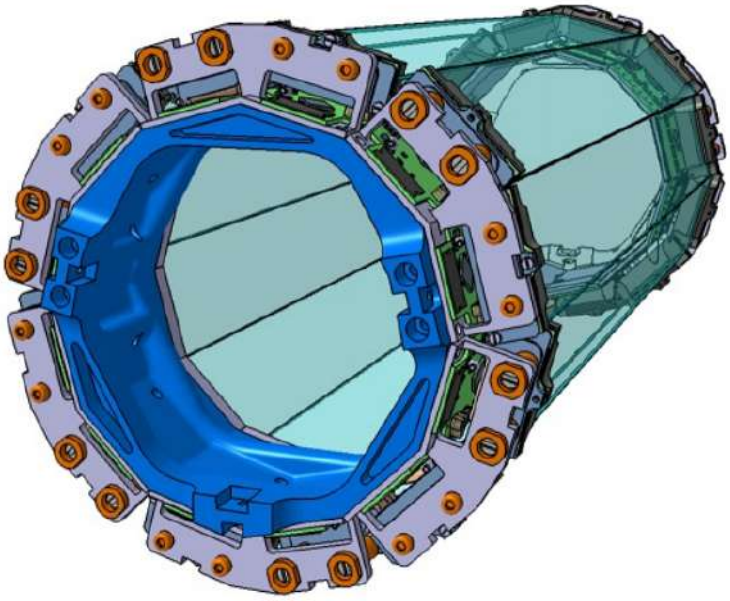

Figure 2.10: Overall structure of the SciFi detector.[14]

2.6 The Scintillating Tile (SciTile) Detector

Another ToF sensor called SciTile detector is located on the inside of the pixel stations in both the upstream and downstream deflection stations.
This detector is made of plastic scintillator material, and since this is the last detector of the particles, there is no longer a need to keep the material budget as low as possible and therefore, there is no longer a limitation on the thickness of the detector. Without this limitation, this detector has the possibility to achieve a time resolution of 23.3 ps.
The readout is done similarly to that of the fiber detector[8].

Chapter 3

Characterization of the micro-twisted pair cables

3.1 The micro-twisted pair cable

Micro-twisted signal cables are used for data transmission from the Vertex and SciFi detectors. One Vertex detector uses 48 pairs of raw micro-twisted signal cables, while one SciFi detector uses 36 pairs of cables[25],[26].
These cables are used for two reasons. Firstly, their low mass helps to minimize multiple scattering [27]. Secondly, they enable high-speed data transfer, which is required for the planned experiment[28],[8].

The micro-twisted pair cables are used to connect the detectors to the Front-end board (FEB) and thus to the DAQ system, which is responsible for the data evaluation of the experiment.
This connection involves data connections from the detector to the Detector Adapter Board (DAB) and a clock connection in the opposite direction. The data connection runs at a speed of 1.25 Gbits^{-1}. In addition, the Vertex detector operates at a clock frequency of 125 MHz and the SciFi detector works at a speed of 625 MHz[13].
The manufacturing process of the micro-twisted pair cable, as it will be utilized in the Mu3e experiment, will be described in this section.

3.1.1 Raw micro twisted signal cables

Micro-twisted pair bundles are differential cables supplied on a coil by Hermann GmbH.
The characteristic of the ordered cable is as follows:
The differential cable consists of two copper pairs with a diameter of 0.127 mm which are insulated with a layer of polyamide that is 0.025 mm thick.

Additionally, the cables have a self-bonding feature due to a 0.010 mm wide aromatic polyamide section. The twist length of the two copper cables ranges from 8 mm to 12 mm[29].
Figure 3.1 shows a newly ordered signal cable coil.
The same type of cables with identical specifications were previously purchased from the same company for the Compact Muon Solenoid (CMS) experiment.

The raw micro-twisted signal cable is often referred to as wire in the following sections to avoid confusion with the micro-twisted pair cable.

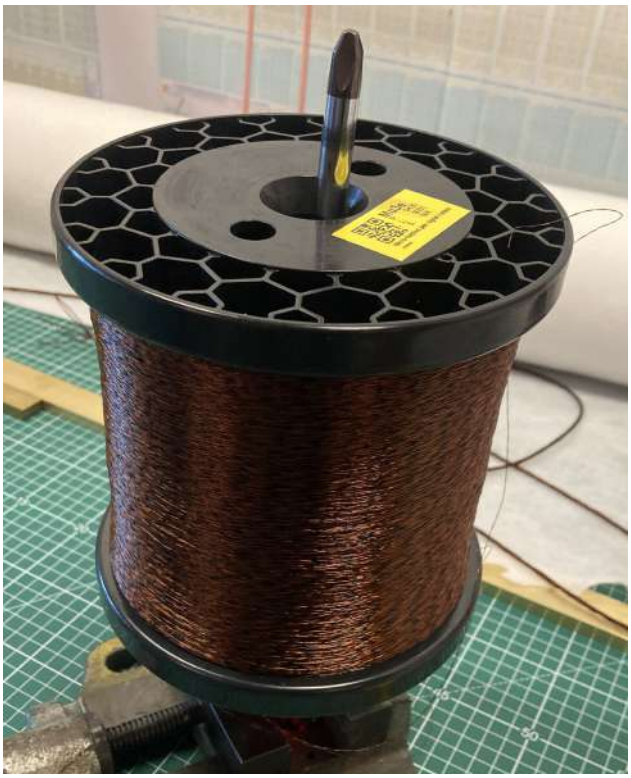

Figure 3.1: A coil for the raw micro twisted cable used for the Mu3e experiment.

3.1.2 Micro twisted pair bundles

The cables are bundled with 50 turns and a length of 1.4 m on the rope machine at PSI[26]. This rope machine twists 6 mini bundles together, while at the same time, the mini bundles, of up to 8 cables per bundle, are twisted into themselves.
Note that the Vertex detector requires cables made of 33 and 44-pair bundles, while the SciFi detector requires cables made of 36-pair bundles[25].
Figure 3.2 shows a micro-twisted pair cable directly after bundling in the rope machine.

To allow the cables to be connected to other devices, adapter boards are soldered on both

ends of the cable.
On one side are the DAB-STP adapters, and on the other, the BoSSLs.
The Detector adapter board - shielded twisted pair (DAB-STP) adapter board is designed to accommodate up to 12 pairs of signal cables, enabling a streamlined connection process. The differential cables are soldered to the board. The connection with another element is then simplified by the plug-in interface of the DAB-STP adapter. Figure 3.3 shows a schematic of the DAB-STP adapter from two sides.
The Adapter Board for Signal, Slow control and Low & high voltage for the vertex detector (BoSSL) is designed to connect the micro-twisted pair cables and the low and high voltage supply via an interposer to the endpiece flex, which is later connected to the vertex detector in the Mu3e experiment[13]. The special shape of the adapter makes it possible to make the connection to the cylindrically arranged ladder as space-saving as possible.
The Vertex detector's cables are connected to either three (for the 33 pair bundles cable) or four (for the 44 pair bundle cable) DAB-STP adapter boards on one side, and two BoSSLs on the other side[25].

Two SubMiniature B - micro-twisted pair (SMB-utp) adapters are attached on both sides for the SciFi detector micro-twisted pair cables, which should fulfill the same functions as the adapter boards of the vertex detector cables[13].
As planned, an external company will partly do the soldering work to connect the cables to the adapters[25].

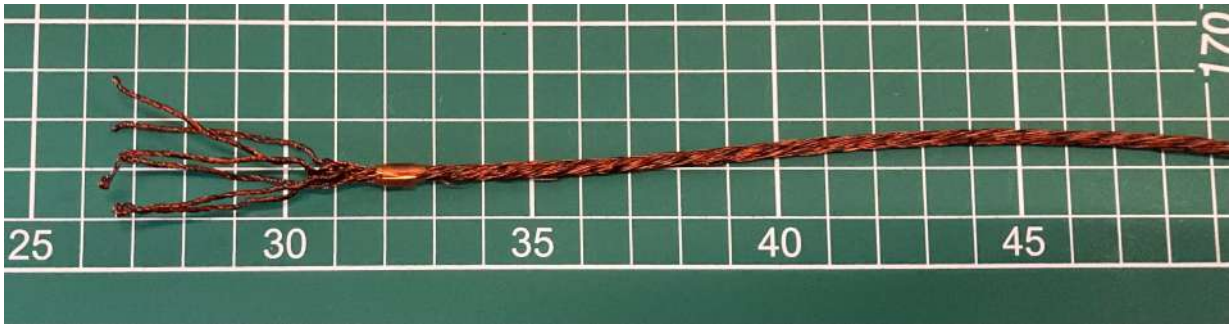

Figure 3.2: Micro-twisted pair cable directly after bundling in the rope machine

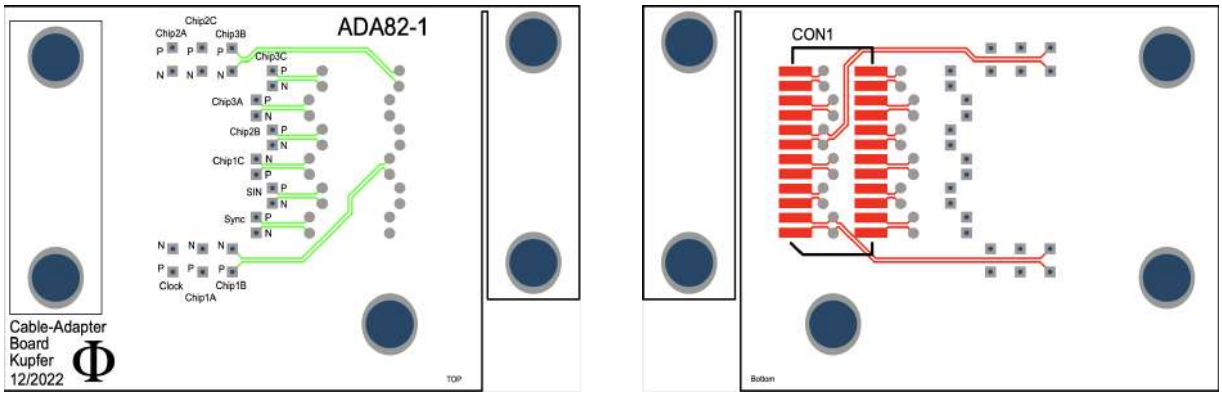

(a) Front-side (b) Back-side

Figure 3.3: The schematics of the DAB-STP Adapter Board from the front- and back-side. On the front side, the points where the cables are soldered on are visible in gray on the left side. and on the back-side, the plug connection, which is connected to all soldered cable pairs, is shown in red on the left side.

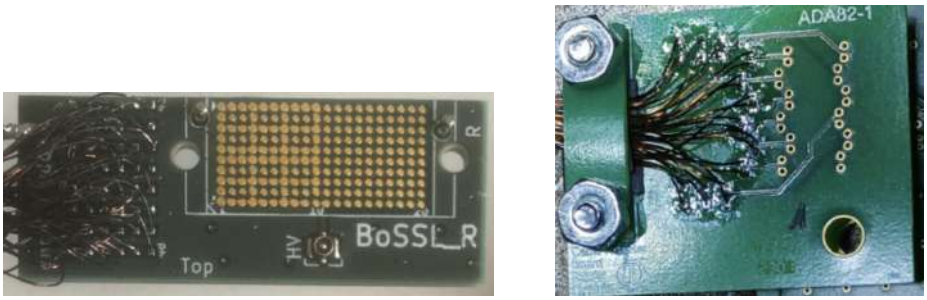

(a) (b)

Figure 3.4: (a) BossL-R Adapter Board (b) DAB-STP Adapter Board

3.2 Measurands for characterizing the cable

There are many different ways to characterize micro-twisted pair cables and check their quality. The following were carried out for the micro-twisted pair cables.

3.2.1 Impedance

The electrical impedance is the electrical resistance in Alternating Current (AC) technology. It is measured in ohms.
As with resistance in Direct Current (DC) technology, impedance indicates the relationship between voltage and current, but in contrast to the DC circuit, these values change periodically in the AC circuit. The impedance is made up of ohmic, inductive, and capacitive resistance:

Ohmic resistance: This is the resistance in the DC and is determined by the material.

Inductive resistance: This is caused by induction in a conductor and is proportional to the frequency of an AC.

Capacitive resistance: This is created by the capacitance in a conductor and is inversely proportional to the frequency of an AC.

It is extremely important for signal transmission in a cable that the impedance of the cable matches the impedance of the system.
If the impedance of the cable does not match the system impedance, reflections will occur. This is because when a signal arrives at the boundary between two different impedances, a part of the signal is reflected back. This can lead to insertion loss, distortion, and interference[30],[31].
Therefore, correct impedance matching is important to minimize reflections and ensure efficient signal transmission. The experimental Setup of the Mu3e Experiment is designed for 90 Ω[13].

The impedance measurement can, therefore, already be used to draw conclusions about the cable's ability to transmit signals.
Furthermore, if the impedance also shows some points that deviate significantly from the average value, it can be assumed that there is physical damage at this point, such as a kink or similar[32].

3.2.2 Insertion Loss

The Insertion loss is the attenuation of the signal power during a transmission line, in the case of this experiment, a differential line of the micro-twisted pair cable. The attenuation is usually expressed in decibels or percent of the inserted signal[33].
There are several factors that cause insertion loss, including:

Ohmic loss: This is the loss due to the resistance of the cable. The longer the cable, the bigger the loss[34].

Losses at connectors and splices: These are the losses direct at the places where the signal enters or leaves a medium, for example, a cable. This can be the reason that there is a mismatch between the impedances or that the connectors are not perfectly connected[35].

The insertion loss says a lot about the transmission quality of a cable.
Firstly, a high insertion loss over all frequencies can cause a decrease in the signal strength, making it difficult to distinguish from background noise and ultimately leading to data loss. Secondly, a high insertion loss difference between frequencies can lead to signal distortion. This is because the insertion loss is expected to be greater at higher frequencies than at lower frequencies, and therefore, the original rectangular signal can take on a shape that cannot be interpreted by the receiver anymore[36].

3.2.3 Crosstalk

Crosstalk is the phenomenon in which transmission on one cable pair results in a signal change on another cable pair. This happens due to overlapping of the electric fields[37]. There are a lot of factors that can contribute to the crosstalk, including:

Coupling length : The longer the cables are parallel to each other, the bigger the effect[38].

Track Separation: The closer the conductors or transmission lines are to each other, the bigger the crosstalk[38].

A distinction can be made between Near End Crosstalk (NEXT) and Far End Crosstalk (FEXT). NEXT corresponds to the crosstalk received on the transmitter side, and FEXT corresponds to the crosstalk received on the receiver side[39].

If the crosstalk is significant compared to the actual measured signal at the receiver, this could lead to signal distortion and, therefore, to transmission errors.

3.2.4 Bit Error Rate (BER)

The BER is a measure of how many bits in a digital transmission were incorrectly interpreted after being transmitted through the cable. It is calculated as the number of erroneous bits divided by the total number of transmitted bits[40].
This particular parameter is crucial for determining the transmission quality of a cable, as it directly reflects the quality of transmission in a given environment.

The BER provides direct information about the transmission quality of the measured cable and can, therefore, confirm the functionality of a cable.
But, in the case of any bit errors, however, the rate does not in itself exclude the cause of these errors. Even with a cable that has no bit errors, it is unclear how good the transmission quality actually is and how robust the transmission quality is against external influences. Further measurements are necessary for this.

3.2.5 Eye Diagrams

An eye diagram is a graphical representation of a digital signal's quality and characteristics of the cable. It is created by superimposing multiple segments of the signal waveform corresponding to individual bit periods. The resulting pattern resembles an "eye," with an open central region.
With this eye, there is the possibility to analyze a lot about the signal quality, including:

Eye opening width: This is the most important information about the transmission quality in the eye diagram. It indicates how good the voltages are, and therefore, the bits are separated from each other. A big eye-opening width makes it easier for the receiver to interpret the bits correctly.

Rise and Fall times: The slope gives insight into the speed of the signal transmission between the bits.

Noise: The noise in the diagrams reflects challenges in the overall signal quality.

Eye diagrams are particularly interesting because they are created comparatively quickly and can, therefore, be used to investigate changes in signal quality with different settings or test setups.

Figure 3.10a shows a representation of an eye diagram.

3.3 Methods to improve the signal quality

There are various methods for improving the signal quality of bit transmissions. In the context of this thesis, the focus was limited to pre-emphasis on the transmitter side and the equalizer on the receiver side. This is because these two methods are also available in the Mu3e experiment.

3.3.1 Pre-emphasis

Pre-emphasis is a signal transmission technique at the sender of a signal that involves increasing the voltage by a fixed pre-emphasis value when the transmission changes from 0-bit to 1-bit. After the first 1-bit, the voltage is decreased by the same value for any further possible 1-bit until the next 0-bit. The process is also applied in reverse when there is a change from a 1-bit to a 0-bit.
This technique results in a faster voltage change for bit changes, leading to a greater signal difference between the two voltages.
The process of pre-emphasis is considered necessary in signal transmission if there is a large insertion loss, especially at high frequencies. Without insertion loss, the signal would be transmitted as a square wave signal, which corresponds mathematically to an infinite series of sinusoidal functions with different frequencies. However, due to the characteristics of a cable with friction and insertion loss, the sine functions with high frequencies are strongly attenuated. Pre-emphasis helps to correct this by amplifying the high-frequency waves, thereby partially compensating for the attenuation.
However, if the pre-emphasis value is too high, the insertion loss may become overcompensated, leading to a deterioration in signal quality[41].

3.3.2 Equalizer

In the equalizer, all the different frequencies are evaluated on the receiver side using a Fourier transformation, and then the signal strengths of the measured frequencies are amplified the higher the frequency. This is because a greater signal loss is expected at higher frequencies due to friction.
Afterward, the equalizer carries out a second Fourier inverse transformation[41].
It is also important to find the correct level for the equalizer before starting the experiment to compensate for the loss of higher frequencies optimally. If the equalizer is set too high, this will also result in an incorrect waveform, leading to bit errors.
Mathematically speaking, this also has the effect of amplifying high signal frequencies, as with pre-emphasis.

As the equalizer takes place after the data transmission, this is not shown by the measurement of the eye diagrams at the end of the transmitting cable.

3.4 Measurement Instruments

For the measurements of the measurands in section 3.2, the following two instruments were used.

3.4.1 Vector Network Analyzer (VNA)

A VNA is a versatile electronic test instrument used to analyze and characterize the electrical performance of high-frequency and radio-frequency devices, circuits, and components. In this experiment, we use a VNA of the type Rohde & Schwarz ZNL14 to measure the impedance and the insertion loss.

Measurement of the impedance with the VNA

For this measurement, the VNA generates a known differential Signal and sends it through the differential cable. When the impedance of the Cable does not match the impedance of the transmission line of the VNA Z_0, there are some reflections in the cable. The VNA measures these reflections and calculates from there the reflection coefficient Γ, which is just the amount of signal amplitude reflected in the cable. Directly at the VNA the device is able to calculate the differential Impedance Z_{diff} with the Formula[42],[43]:

$$Z_{diff} = Z_0 \frac{1+\Gamma}{1-\Gamma} \tag{3.1}$$

For a measurement on specific points on the cable L meters from the VNA, the phase of the magnitude of a reflection will be shifted by an amount based on the electrical distance $\phi = 2\pi L/\gamma$, with γ the wavelength. The coefficient Γ' at this point will be: $\Gamma' = \Gamma e^{-i2\phi}$. Using this formula together with equation 3.1, the VNA is then able to measure the impedance at any point on the cable[43].

Measurement of the insertion loss using the VNA

The VNA measures insertion loss by sending a signal with a known frequency from one port and measuring the received signal at the second port. The insertion loss is then calculated as the ratio of the received signal to the transmitted signal. This measurement requires both ports of the VNA.
The VNA repeats the insertion loss measurement at different frequencies, which can be chosen before.

3.4.2 Serial Data Analyzer (SDA)

A SDA is a type of test and measurement instrument designed to analyze and troubleshoot serial data communication systems. It is commonly used in the field of electronics and

telecommunications to examine the quality and integrity of digital signals transmitted serially.
Here the SDA is used to measure the eye diagrams.

Measurement of the eye-diagrams using the SDA

The serial data analyzer measures eye diagrams using a process that involves clock recovery and data segmentation, which works as follows[44]:

Clock Recvovery: The SDA uses a method called Phase-Locked Loop (PLL) to learn the clock period. To do this, the oscillator in the SDA generates a periodic signal, and a phase detector compares this periodic signal with the periodicity of the measured input signal. The phase detector adjusts then the phase of the signal until the phases are matched and, therefore finds the correct frequency. If the frequencies are identical, it is said that the PLL is locked.

Data Segmentation: With the determined clock period, the data record can than get divided into segments somewhat larger than the clock period.

Persistence Display: With the recovered clock, the segments are overlayed in a persistence display.

The SDA can then read out some values such as the eye-opening or the amplitude of the eye, directly from the measurement.

3.5 Method

3.5.1 Impedance Measurements

The impedance of the cable is measured using the VNA and the Mu3e cable diagnostic card, which can be seen in Figure 3.5. This diagnostic board makes it possible to access all cables soldered to the DAB-STP adapter via simple connections.
The two connection cables of the VNA should be connected via the diagnostics board to measure the desired differential cable pair of the micro-twisted pair cable.

It is expected to measure significant fluctuations in impedance during the measurement for the first few centimeters. This is due to the fact that the diagnostic board and the DAB-STP adapter come into contact at this point. Since it is only a simple plug connection, a partial contact could be expected, which results in impedance fluctuations[45]. However, this part of the measurement is not yet interesting, as the measurement wants to investigate the impedance of the cable and is not interested in the impedance of the board and its connections. Because of that, actual measured values for calculating the mean impedance of the cable were only collected after 20 cm.
After the end of the cable, the impedance is expected to increase to infinity as the end of the cable is left open[46]. The measurement is, therefore, stopped after one meter to calculate the average value.
Since the distance on the diagnostic board is different for different differential cable pairs, the cables appear to have different lengths in the measurement.

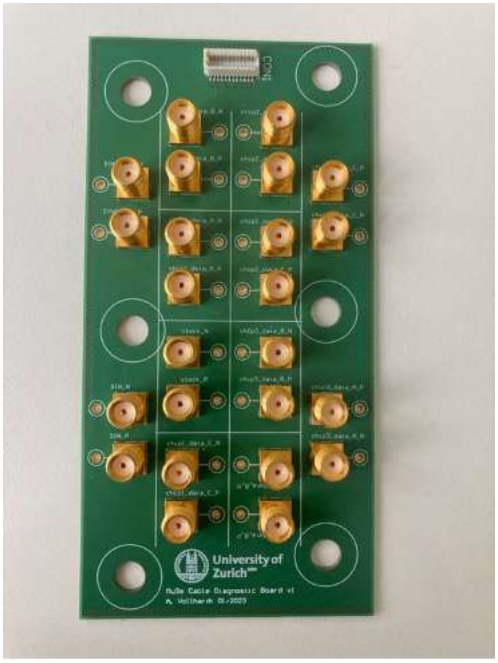

Figure 3.5: The Mu3e diagnostics board. It connects the various cables of the micro-twisted pair cable directly to the cable connections on the board via the DAB-STP adapter connection, which is shown on top.

3.5.2 Insertion Loss Measurements

In order to accurately quantify the amount of insertion loss in a system, it is necessary for the measuring instrument - in this case, the Vector Network Analyzer (VNA) - to have the capability to both generate the input signal and measure the output signal. Additionally, it should be noted that the diagnostic board, which was previously utilized to measure impedance, can no longer be utilized to measure the insertion loss, as the VNA, which only has two connections, cannot be differentially connected on both sides of a differential cable.

Therefore, for the insertion loss measurement, the "Mu3e Cable Diagnostic Board v1 Balun", shown in Figure 3.6, is used. This board has a TCM-2-33X+ type balun at each connection point, which converts a balanced line system to an unbalanced one and vice versa.
According to the manufacturer, the balun is designed for frequencies between 30 MHz and 3000 MHz and has an insertion loss between 1.5 dB and 3 dB and a return loss between 19 and 28 dB[47].

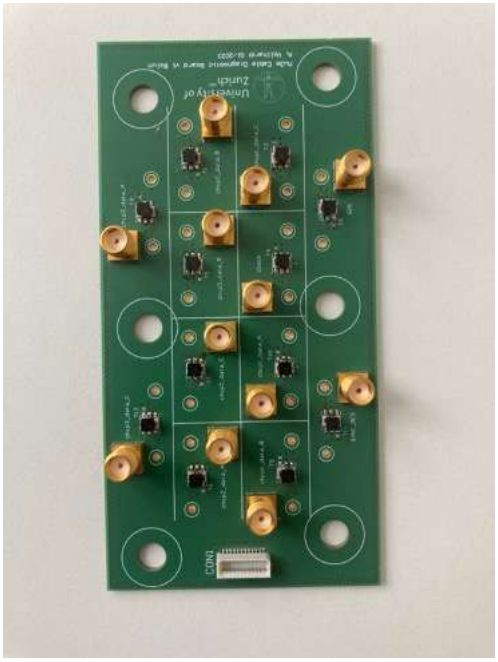

Figure 3.6: The Mu3e diagnostics board with a balun, which connects a differential cable pair from a balanced line system, connected over the DAB-STP adapter into a symmetrical unbalanced single line system on the board.

Unbalanced Line System: Signal transmission occurs through a voltage that changes the reference potential.

Balanced Line System: Data is transmitted through a pair of identical signal conductors, with the signal on one conductor and a reference signal on another. This makes the entire signal more immune to interference, as much of the noise dissipates during the differential process.

As the cable can only be connected to the diagnostic board via the DAB-STP connectors, it is impossible to connect the cable on both sides to the VNA.
Therefore, the signal at the end of the cable, at the BoSSL (-L or -R), is rerouted from one differential cable pair to another using a loopback card, which is placed directly on the pads of the BoSSL via an interposer. The signal then arrives at another connection at the same end of the cable as it was sent and gets routed through the balun on a connection point of the diagnostic board, where it can be read out by the VNA.
In the end, the insertion loss in dB is divided by two to get the insertion loss of one cable length.
The results are then divided by the cable length to get the insertion loss per meter, which makes it easier to compare.

To determine the length of each cable, an impedance measurement was conducted. The distance was determined by measuring the point where the impedance exceeds 110 Ω and subtracting 20 cm, which is the maximum distance expected on the diagnostic board.
The measurement is performed for signal frequencies from 5 kHz to 3 GHz.

Calibration
When measuring insertion loss, it is important to measure only the loss caused by the cable and its connectors. This is because other insertion losses that occur outside the cable, such as those caused by the balun or the diagnostic board and the connection between the VNA and the diagnostic board, will not be present in the experiment. In order to exclude these losses from the result as far as possible, a calibration was designed.
Since the balun has a large insertion loss, which is also strongly frequency-dependent[47], the calibration should also be dependent on the frequency.
To do this, on a new DAB-STP, a pair of differential connections are interconnected using two wires. This "bridged" DAB-STP is shown in Figure 3.7.
The insertion loss of the adapter at different frequencies connected to the Diagnostic Board with balun was measured using the VNA.
To compensate for insertion loss outside the cable, in later measurements, this calibration measurement, in dB, was subtracted from each measurement of differential cables from the micro-twisted pair cables for each frequency.
However, it is important to note that the insertion loss in the BoSSL with the loopback card is not calibrated away with this setup. However, due to the short distance the signal has to travel through the loopback card and the interposer, this insertion loss can be expected to be negligible.
Figure 3.8 shows the measured insertion loss of the system with the "bridged" DAB-STP adapter.

Fundamental Frequency
The fundamental frequency or maximum data frequency corresponds to the maximum frequency in a cable at which data can be transmitted. In a cable that transmits binary data, such as the micro-twisted pair cable, this frequency corresponds to the alternating transmission of the 0- and 1-bit, which is half the data transmission rate. Higher frequencies no longer allow data transmission[48]. As this frequency is important for data transmission, it is particularly interesting to compare the insertion loss at this frequency.
The fundamental frequency of a cable with the data rate of the Mu3e experiment, which is 1.25 Gbits^{-1} is therefore a frequency of 625 MHz.

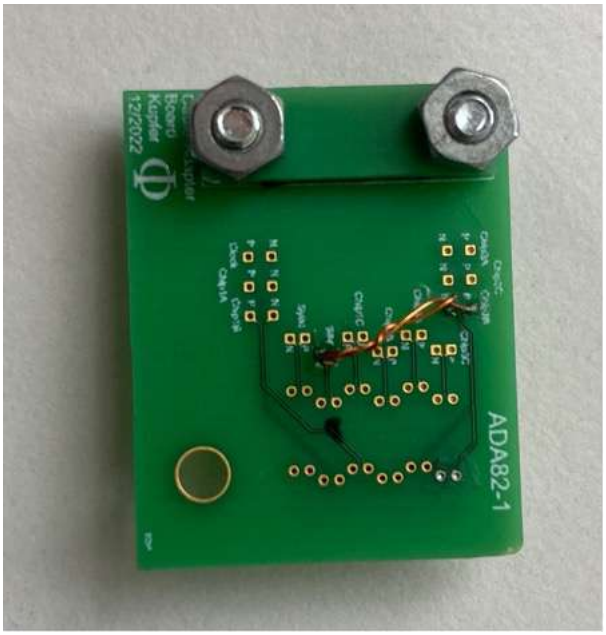

Figure 3.7: The DAB-STP adapter in which a copper wire bridge directly connects two pairs of cables. This was done to calibrate for insertion loss happening outside the micro-twisted pair cable.

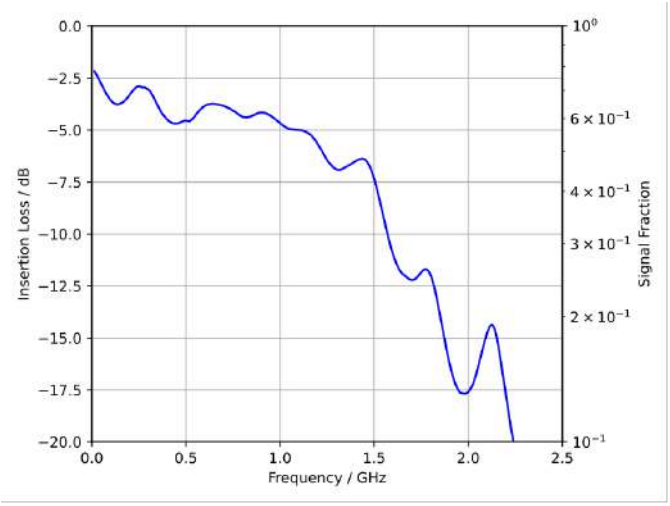

Figure 3.8: The measured insertion loss values for various frequency points obtained during measurement of the bridged DAB-STP adapter. This measurement will be subtracted from any other measurement in the future in order not to include the insertion loss due to the diagnostic board and the DAB-STP adapter in the measurement.

3.5.3 Crosstalk Measurement

The same arrangement, inclusive calibration, used for measuring insertion loss is applied to measure crosstalk. The only difference is that the signal is measured on a differential cable pair that is not connected through the loopback card to the cable pair through which the signal was initially transmitted.
As the loopback card is still used in this measurement, a superposition of the two crosstalk types (NEXT and FEXT) is measured here.

The signal component measured is then analyzed similarly to the insertion loss measurement at different frequencies.
The mean value of the crosstalk is evaluated for all values between 200 MHz and 2 GHz.

3.5.4 Bit Error Rate (BER) Measurements

The measurement of the BER when communicating with the micro-twisted pair cable is carried out with the following setup:
A Cyclone V GX Starter Kit Front-end board (FEB) is connected to a differential cable pair of a micro-twisted pair cable using the diagnostic board, which was also used to measure the impedance and is shown in Figure 3.5. This FEB is, in turn, connected to the computer.
In contrast to the custom-developed FEB on the Mu3e Experiment, this FEB directly supports the possibility of amplifying FEB signals with a pre-emphasis and improving signals arriving at the FEB with an equalizer.
On the other side of the cable, the BoSSL is connected to an endpiece flex, which routes the cables to a pad, as planned later in the Mu3e experiment.
Contacts were then soldered to contact points on this pad of the endpiece flex. Over these contact points, the same cable pair of the micro-twisted pair cable is then connected to the FEB again.
The endpiece flex, which has two soldered contact points, is shown in Figure 3.9.
With this setup, the cable with the endpiece Flex was now connected to the FEB on both sides, which now allows the transmission and measurement of bit sequences.

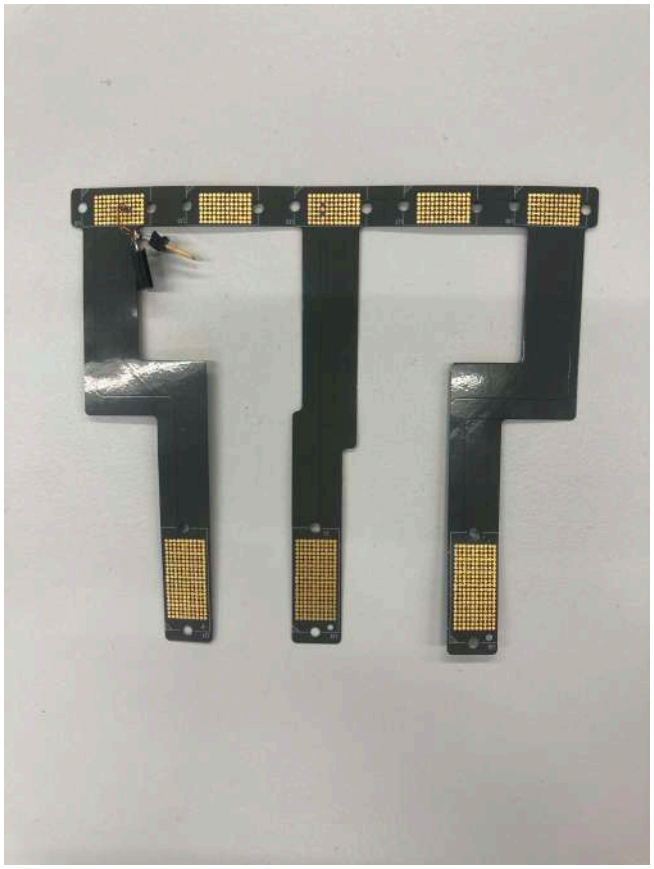

Figure 3.9: The endpiece-flex for a downstream cable with contact points soldered to two pads.

Individual bit sequences of 7 bits are now generated on the front-end board. The 1 bit corresponds to a freely selectable positive voltage of the signal level, and the 0 bit corresponds to the same negative voltage.
At the other end of the cable, the voltage is measured again by the FEB, and each bit is getting interpreted.
The BER indicates how many of these bit combinations, consisting of 7 bits, are correctly interpreted by the FEB.
The data rate denotes the number of bits transmitted per second and can be flexibly adjusted on the FEB. In this particular case, the data rate was chosen to be $1.25\,\mathrm{Gbits}^{-1}$ to align with the maximum bit rate at the Mu3e experiment.

With the FEB in this Experiment, the value of the pre-emphasis can be chosen freely, and the value of the equalizer can be differentiated between two levels and a complete switch-off.

3.5.5 Eye diagram Measurements

To obtain eye diagrams, bits are produced the same way as for the BER and transmitted through the cable. However, the signal received at the endpiece flex is now measured at the same contact point where a contact has already been soldered to determine the BER. The measured voltage is then measured with the SDA and superimposed for all the measured bits.
Figure 3.10 displays the eye diagram of a cable measurement with a signal level of 220 mV. Figure (a) depicts the measurement without pre-emphasis, and Figure (b) shows the measurement with a pre-emphasis of 44 mV.

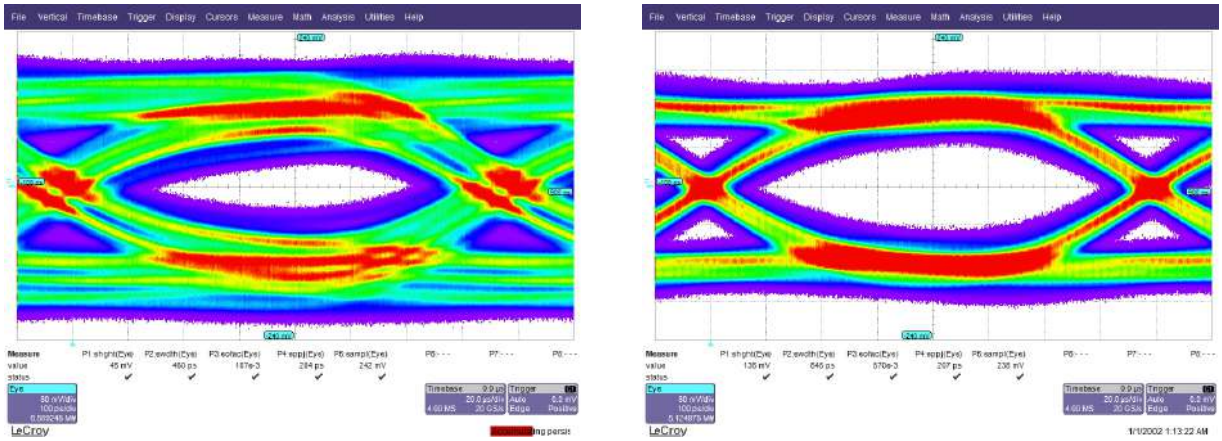

(a) (b)

Figure 3.10: The representation of the eye diagrams for measuring the cable used in the Mu3e experiment and the endpiece flex. A signal level of 220 mV was selected without pre-emphasis in (a) and with a pre-emphasis of 44 mV in (b).
In (a) 6.59×10^6 and in (b) 5.12×10^6 single bit measurements were superimposed.
On the horizontal axis is the time in picoseconds, and on the vertical axis is the measured voltage in millivolts.

The SDA now evaluates some values on the eye diagrams.
The eye height and eye width correspond to the width and height of the "eye", i.e., the width and height of the opening in the center.
The eye amplitude corresponds to the maximum and minimum measured voltage difference.
The eye height, given as a percentage of the eye amplitude, is called the eye-opening factor.
The jitter corresponds to the time fluctuation in the rise and fall sequences.
In a measurement without insertion loss, these measured values would describe a rectangular function, i.e. no jitter and maximum eye size. However, since this is never found in reality, the goal is to attempt to select the pre-emphasis in such a way that the measured values are optimized as much as possible at a fixed signal level.

3.6 Result

Two vertex cables made from the new coils (called Mu3e coils) were available for the measurement. These cables are fully equipped with 4 DAB-STP boards and two BoSSLs on the other side.

Furthermore, a cable from an old coil, called CMS coil, ordered in the past by the CMS collaboration, was available. This only had one soldered DAB-STP board and one BoSSL.

Three individual wires directly from the coil were also available to measure the impedance and insertion loss. These were soldered directly on both sides to a differential connection on a DAB-STP.

3.6.1 Impedance Measurements

The impedance measurement has shown that for the two cables with wires from the Mu3e Coil, all undamaged wires have an impedance over the entire length between 70 Ω and 80 Ω. The average values of the two cables are 73.88(69) Ω and 73.72(52) Ω respectively. For an example of such an measurement see Figure 3.11, which displays the impedance measured at different distances in one wire.

The Cable with wires from the CMS coil showed an average impedance of 92.27(324) Ω.

Figure 3.12 illustrates the measured impedance for a raw signal cable from the CMS coil and two newly ordered Mu3e Coils. The impedance of the raw cable from the CMS coil was measured at 96.64(284) Ω. Meanwhile, the impedance of the two newly ordered coils was measured at 78.21(192) Ω and 78.17(170) Ω, respectively.

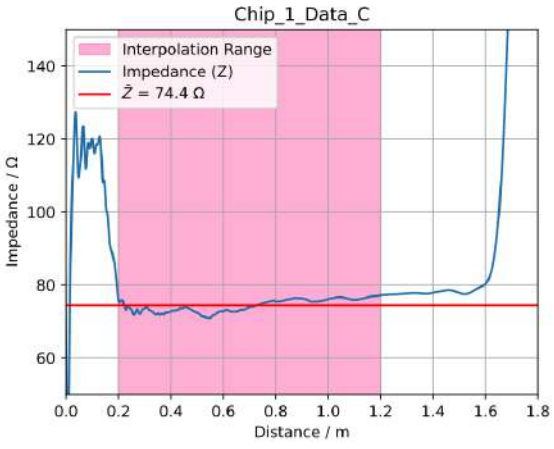

Figure 3.11: Measurement of the impedance of a pair of cables. The measurement of impedance is graphed against the distance of the cable pair. The range over which the mean value was calculated is shown in pink.
This measurement was made for the DAB-STP-0 adapter of cable 0450-0001-0000002.

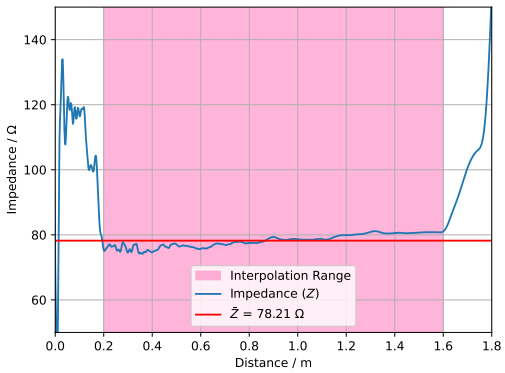

(a) Mu3e coil 1

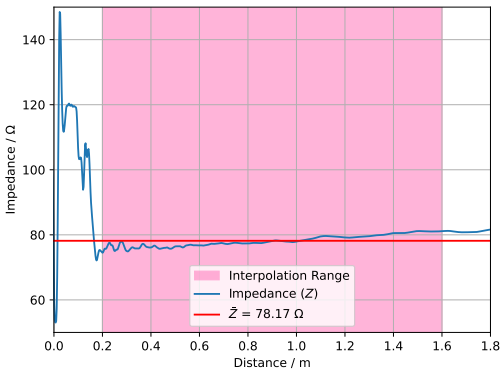

(b) Mu3e coil 2

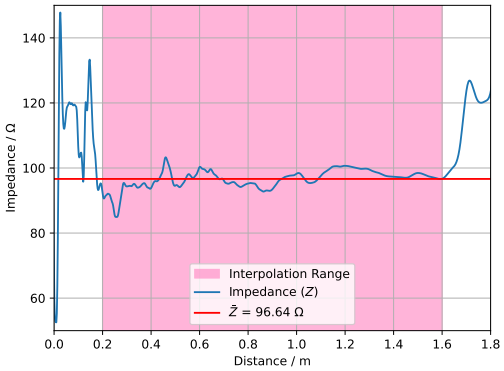

(c) CMS coil

Figure 3.12: Impedance measurements which were taken for individually stripped cable pairs across three distinct coils - two newly ordered Mu3e coils and one CMS coil ordered by the CMS collaboration in the past.
The distance and corresponding impedance values were graphed against each other. The range highlighted in pink indicates the interval that was used to calculate the mean value. The two cables from a new coil for the Mu3e experiment exhibit significantly lower impedance than the cable from the coil ordered for the CMS experiment.

The measurement of all cables shows that there are clear differences in the impedance between the cables of the two coils. The differences are over 10%.
This could potentially be problematic as the Mu3e system is designed for an impedance of 90 Ω. Further measurements are necessary to determine the possibility of signal transmission.

3.6.2 Insertion Loss Measurements

The measurement of the insertion loss has shown that for all undamaged cable lines from cables made of Mu3e wires, there is an insertion loss of approximately $4.5\,\mathrm{dBm}^{-1}$ at the fundamental frequency of 625 MHz.
For example, see the measurement of a wire in Figure 3.13. The insertion loss is plotted against the measured frequency.
Figure 3.14 displays the insertion loss measured at 625 MHz for both cables from the Mu3e coil. The mean values are very similar, around $4.3\,\mathrm{dBm}^{-1}$.

Figure 3.15 displays the insertion loss measurements at 625 MHz for the micro-twisted pair cable made of raw cables from the CMS coil. The mean value is $5.18(32)\,\mathrm{dBm}^{-1}$.

Figure 3.16 illustrates the measured insertion loss for a raw signal cable from the CMS coil and two newly ordered Mu3e Coils. Because the cable was soldered on both sides to the DAB-STP adapters, for this measurement, no loopback card was needed.

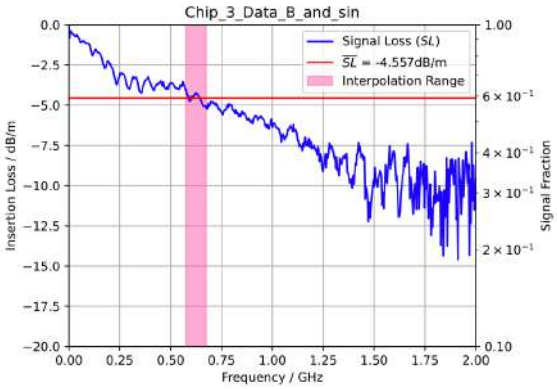

Figure 3.13: Measurement of the insertion loss of two cable pairs. The measured frequency is displayed along with the corresponding insertion loss values in both decibels per meter and percent. The range over which the mean value was calculated is shown in pink.
This measurement was made for the DAB-STP-0 adapter of cable 0450-0001-0000002.

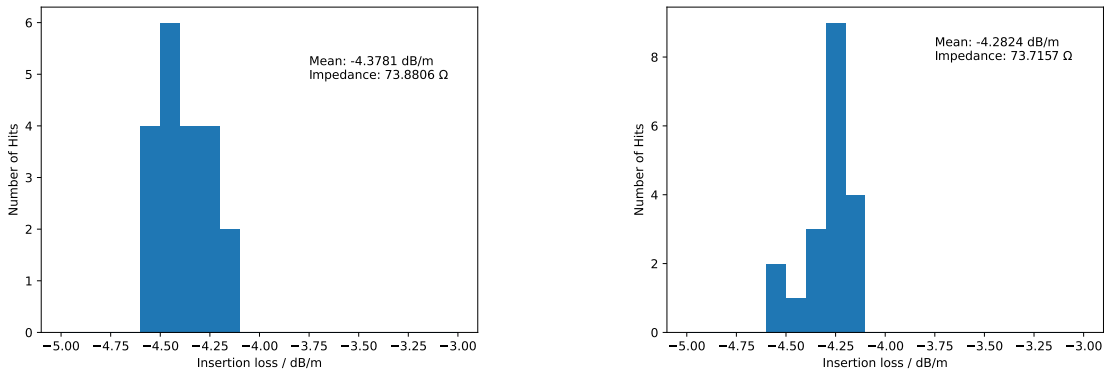

(a) Cable 0001-0002

(b) Cable 0001-0003

Figure 3.14: The results of measuring the insertion loss in dBm^{-1} at a frequency of 625 MHz are presented for two different prototypes of micro-twisted pair cables used for the Vertex detector.
The mean value for the insertion loss for all functioning connections of the respective cable and the mean value for the impedance of all functioning connections are displayed in the top right corner.

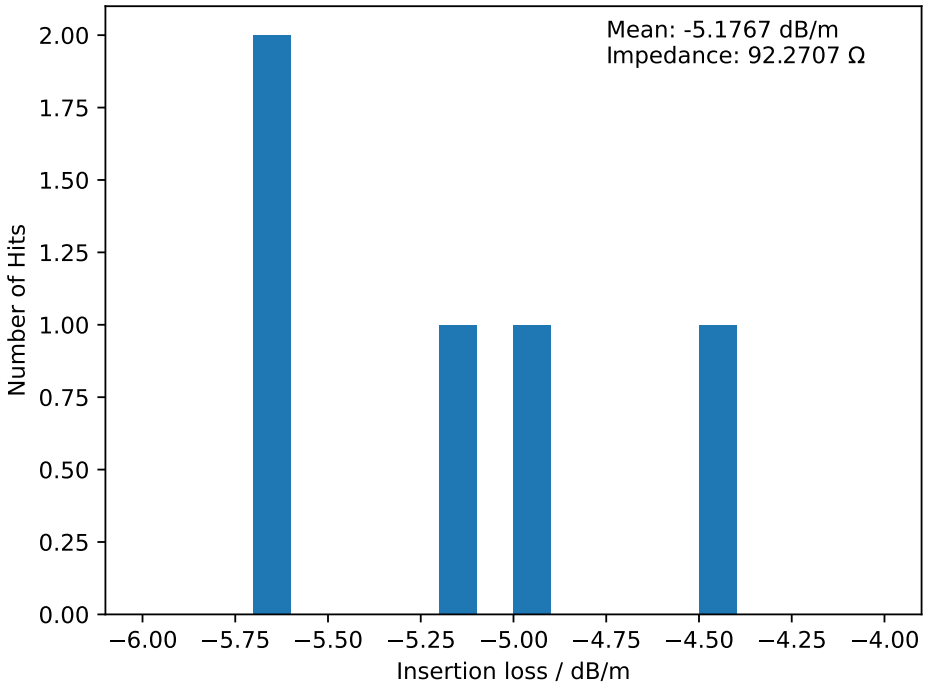

Figure 3.15: The results of measuring the insertion loss in dBm^{-1} at a frequency of 625 MHz is presented for a prototype of a micro-twisted pair cable used for the Vertex detector. The partial cables were selected from an old coil ordered from the CMS collaboration.
The mean value for the insertion loss for all functioning connections of the respective cable and the mean value for the impedance of all functioning connections are displayed in the top right corner.

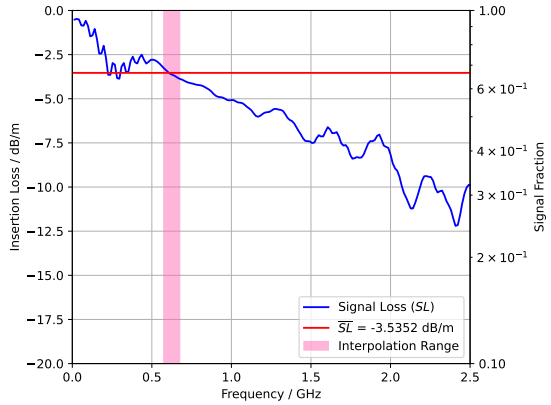

(a) Mu3e Coil 1

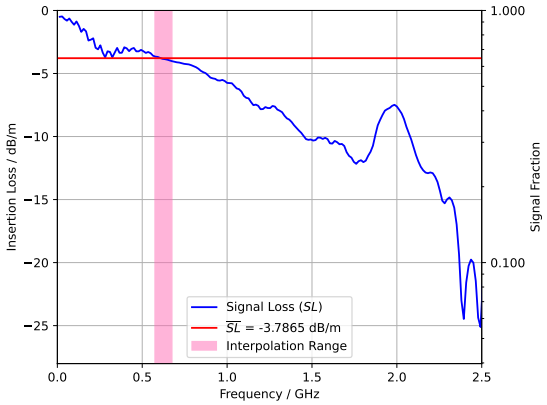

(b) Mu3e Coil 2

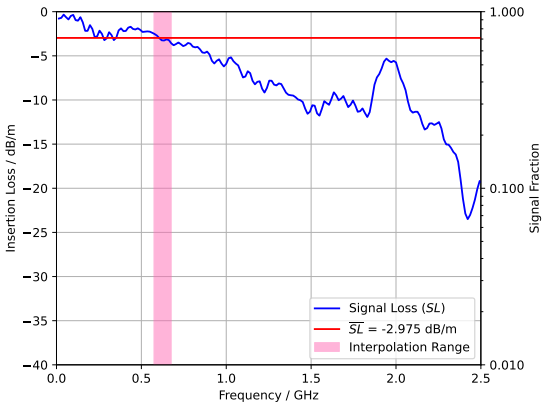

(c) CMS Coil

Figure 3.16: Insertion loss measurement of individually stripped cable pairs for three spools. The distance in meters is plotted against the measured corresponding impedance in ohms. The range in pink indicates the range over which the mean value was calculated.
The cable insertion loss from the Mu3e coil is significantly higher than that of the cable from the CMS coil.

The measurements show differences between the cables. The measurements of the individual stripped cables show a slightly larger insertion loss at the fundamental frequency for the Mu3e wires compared to the CMS wire.
When measuring the cables, this difference is reversed, but it must be noted that due to only one available DAB-STP element and the need for two cable pairs per measurement, only little data is available for the cable made of CMS wires. Furthermore, the cable seemed already damaged, possibly leading to a higher insertion loss.

3.6.3 Crosstalk Measurements

The measurement of the crosstalk, for all three cables, shows that for undamaged cable pairs, the mean crosstalk of a signal attenuated by 30 dB up to 45 dB of the measurement signal is measured, this large fluctuation is explained by the fact that the local proximity of the cable pairs on the micro-twisted pair cable is decisive for the measured value.
See the measurement of a cable pair in Figure 3.17 as an example where the measured insertion loss of the input signal is contrasted with the measured frequency.

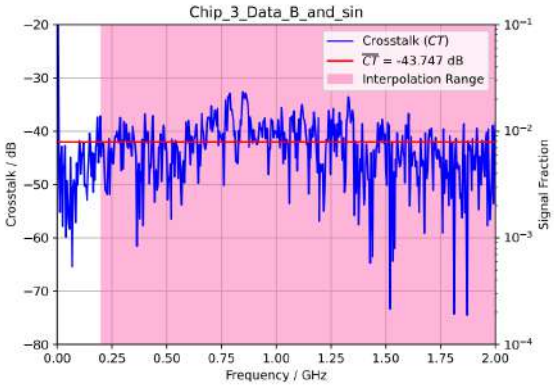

Figure 3.17: Measurement of the crosstalk of two cable pairs. The x-axis shows the measured frequency, and the y-axis is the signal fraction of the inserted signal in dB and in percent. The range over which the mean value was calculated is shown in pink.
This measurement was made for the DAB-STP-0 adapter of cable 0450-0001-0000002.

The measurement shows that the crosstalk measured in another cable is in the order of 1% of the original signal.
But despite the insertion loss in section 3.6.2, a signal level of approximately 50% of the original signal amplitude of the actual signal level is still observed at the end of the cable. According to this measurement, the crosstalk in the micro-twisted pair cable would be about two percent of the measured signal and, therefore, negligible.

3.6.4 Bit Error Rate (BER) Measurements

The cable 0450-0001-0000002 with raw micro twisted signal cables from the Mu3e coil allows for error-free communication for over an hour without any pre-emphasis or equalizer, starting with a signal level of 220 mV. By adding a pre-emphasis of 10 mV, error-free communication for more than an hour was achieved with a signal level of 100 mV.
In contrast, the cable with raw micro twisted signal cables from the CMS coil showed error-free communication at 100 mV without a pre-emphasis.
An equalizer stage can be used on the receiver side instead of reemphasizing the transmitter side to ensure error-free communication. The front-end board specifies the strength of

the pre-emphasis, which is available in two levels. By setting the equalization to level 1, error-free communication at a signal level of 100 mV was also possible with the cable from the Mu3e coil.

In general, it can be seen that error-free communication is possible with both cables, even if the BER differs significantly at lower amplitudes. But for lower amplitudes in the cable with wires from the Mu3e coil, a pre-emphasis or an equalizer is needed.

3.6.5 Eye diagram Measurements

The eye diagrams are measured for the cable 0450-0001-0000002 made of Mu3e wires and the cable made of CMS wires.
The comparison of the two cables revealed a significant difference in their eye diagrams. The cable from the CMS coil exhibited a wider eye-opening than the other cable at the same pre-emphasis level.
The changes in various eye diagram parameters for both cables at a signal level of 400 mV can be observed in Figure 3.18. The percentage of pre-emphasis of the signal level is shown on the horizontal axis, while the values of all parameters are shown on the vertical axis.
The Figure also indicates that about 30% pre-emphasis of the signal level is necessary for optimal eye-opening, which translates to the best transmission quality in the cable.

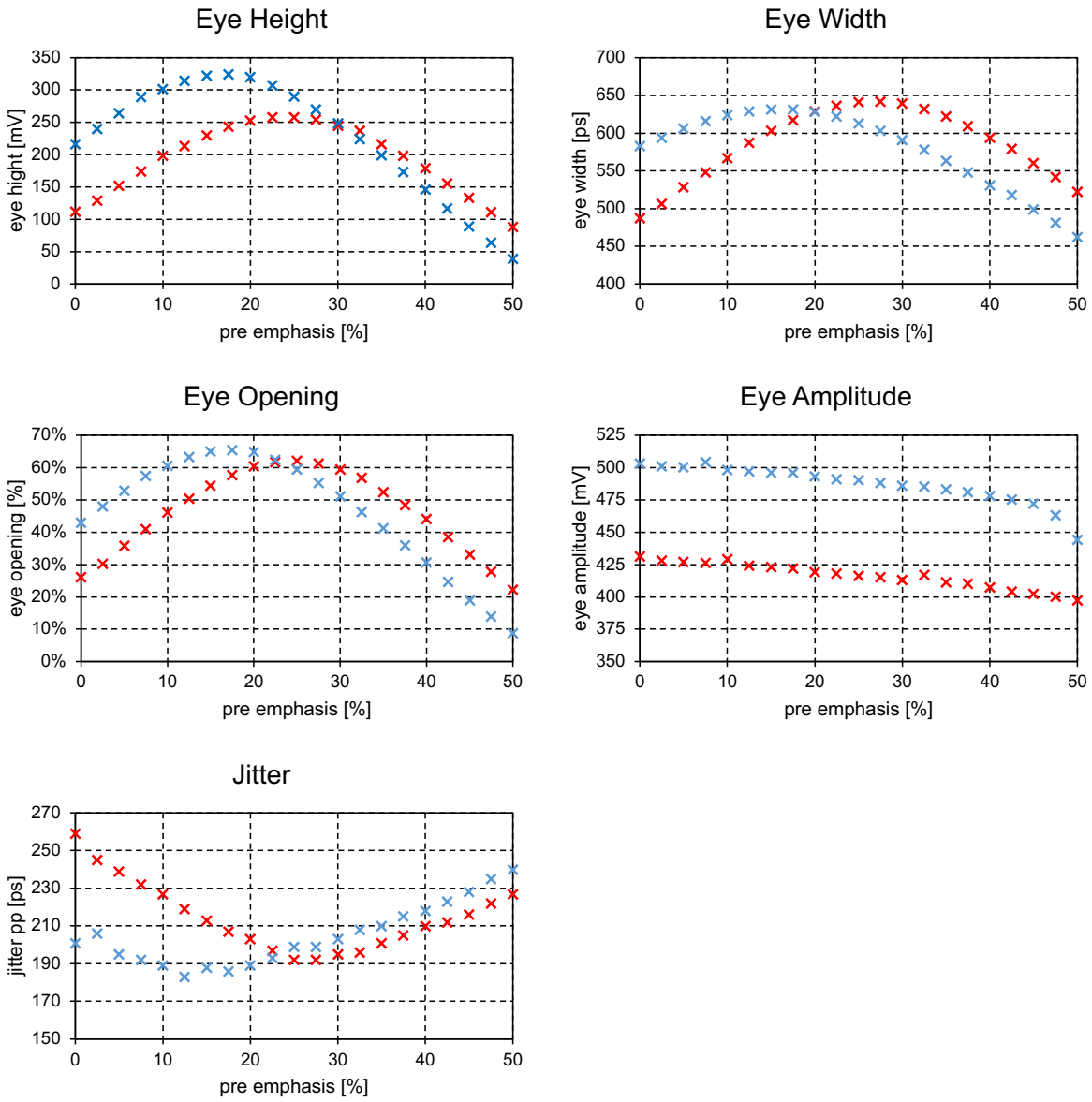

Figure 3.18: The graph displays the various values of the eye diagrams on the y-axis against the pre-emphasis settings on the x-axis, measured in percentage. The signal level selected for the graph is 400 mV. The red line represents the values for the micro-twisted pair cable made of raw cable from the Mu3e coil (0450-0001-0000002), while the blue line represents the values for the micro-twisted pair cable made of raw cable from the CMS coil.
It is noticeable that the cable with lower impedance has a significantly smaller eye-opening, particularly with less pre-emphasis, though the eye-opening can be significantly enlarged with a sufficiently large pre-emphasis.

Based on the data analysis, it is evident that the two cables exhibit a noticeable difference in

their performance. Even though the cable with raw cables from the Mu3e coil has a higher BER and inferior eye diagrams, it is still possible to achieve error-free communication with an adequate eye opening using pre-emphasis.
The technical design of the Mu3e experiment incorporates pre-emphasis on the transmitter side, as mentioned in [13], which is why the cable remains suitable for stable communication at a rate of $1.25\,\mathrm{Gbits}^{-1}$. However, it is crucial to carefully select appropriate values for the signal amplitude and pre-emphasis to ensure optimal performance.
Overall, the results indicate that even though the Mu3e coil wire cable may not perform as well as the other cable, it is still a viable option for stable communication, provided that the appropriate pre-emphasis values are utilized.

3.6.6 Scintilating Fibre (SciFi) Cables

Two prototypes of the SciFi cable were analyzed to validate the measurements obtained in the previous section and gather additional data for the SciFi group. These prototypes were again made of raw signal cables from different coils - Cable 1 is made of cables from a new coil ordered for the Mu3e experiment, while Cable 2 is made of cables from an old coil ordered for the CMS collaboration. Notably, the SciFi micro-twisted pair cables differ from the Vertex cables, as they contain only 36 signal cables and are furnished with SMB-utp adapters at both ends. Therefore, marginally adapted measurement methods are imperative to precisely assess these cables' properties.
A diagnostic board is also available for the SMB-utp adapters, which enables connection to all cable pairs.

Impedance, Insertion Loss and Crosstalk

Method
Impedance measurement
All 24 differential cable pairs were directly connected to the VNA via the diagnostic board to measure the impedances of the cables. The impedance was measured using the same principle as the Vertex cable.
Insertion-loss measurement
However, no special diagnostic board with a built-in balun was available to measure the insertion loss. Hence, an external KDTBARON-003 balun was used to convert an unbalanced line system into a balanced one. Both measurement cables from the VNA were connected to the balun, and both differential connections from the balun were then connected to the respective connections on the diagnostics board.
Unlike the Vertex cable, each signal connection could be measured individually, as the signal could be connected to a diagnostic board on both sides of the cable, and therefore, no loopback card is needed.
To reduce interactions between the baluns which leads to oscillations in the measurements, attenuators of 10 dB were placed on both outputs on the differential side of one balun. Figure 3.19 displays the measurement of insertion loss, both with and without attenua-

tion. This graph shows the necessity of applying attenuation to enhance the quality of the measured signal.
To calibrate the measurement system, a measurement in which the two baluns, including attenuators were directly connected was made. This measurement was then subtracted in dB for each frequency separately, identically as done for the vertex cable.

Crosstalk measurement

The crosstalk was also measured using the same setup as for the insertion loss.

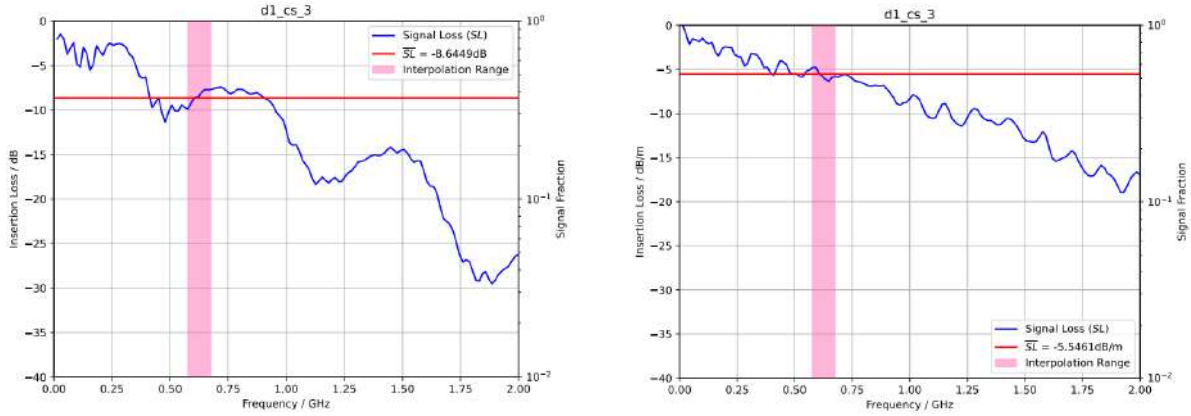

(a) Without attenuation

(b) with attenuation of 10 dB

Figure 3.19: Measurement of the insertion losses on a signal cable of the micro-twisted pair cable, once without and once with attenuation of 10 dB between the two baluns.
On the graph, the horizontal axis shows the measured frequency, while the vertical axis displays the insertion loss, measured both in decibels and as a percentage. The range over which the mean value was calculated is shown in pink.

Result

The **impedance** measurements conducted on the cables used for the vertex detector indicate that they have similar values as those of the vertex cables. The mean impedance values for the cables from the Mu3e coil and the CMS coil were 77.02(90) Ω and 90.84(153) Ω respectively.

Figure 3.20 shows a histogram of the **insertion loss** measurements for the two measured cables for all cable pairs. This measurement shows that the insertion loss of cables made from raw cables from the Mu3e coil is greater than that of cables made from raw cables from the CMS coil. This also supports the result of the individual stripped wires.
However, it must also be mentioned that there are significant differences in the insertion loss values between the measurements of the SciFi cables and the Vertex cables. It can be assumed that the following two reasons are responsible for this. Firstly, a modified calibration had to be carried out for the measurement, which meant that, for example, the loss on the diagnostic board was no longer deducted. Secondly, the SciFi cables, which

have a plug connection on both sides, were also measured differently.
Therefore, the absolute values of the insertion losses should not be compared with the measurements for the vertex cable.

The results for **crosstalk** were very similar to the results from the vertex cables and showed large fluctuations for the same reasons.

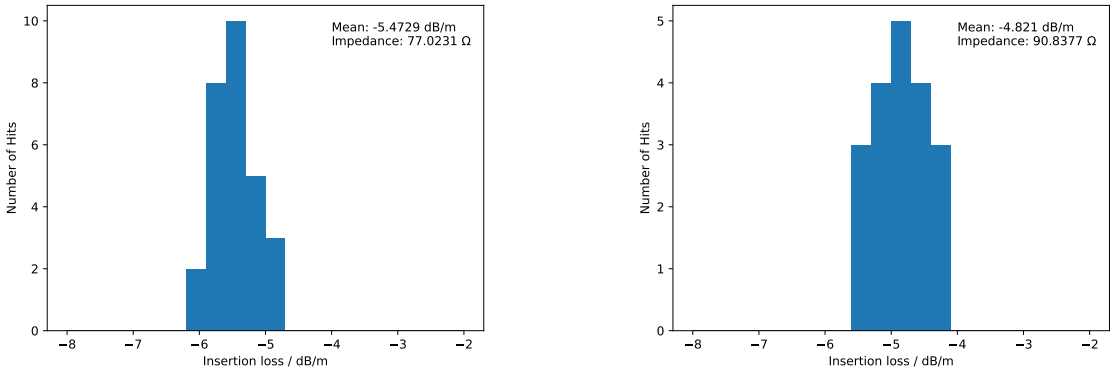

(a) Mu3e Coil (b) CMS Coil

Figure 3.20: The results of measuring the insertion loss in dBm^{-1} at a frequency of 625 MHz are presented for two different prototypes of micro-twisted pair cables used for the Vertex detector. The partial cables were selected from separate coils.
The mean value for the insertion loss for all functioning connections of the respective cable and the mean value for the impedance of all functioning connections are displayed in the top right corner.
The results indicate that the cable with higher impedance had a significantly lower insertion loss than the cable with lower impedance, which was expected based on the cables' measurement results for the vertex detector.

Eye Diagram Measurement

The diagnostic board on both ends of the cable allows for direct reading of the eye diagrams when communicating via SciFi cables, eliminating the need for an additional connection such as an endpiece flex. The measurement setup of SciFi cables is, apart from the endpiece flex, equivalent to that of Vertex cables.
Figure 3.21 displays changes in eye diagram parameters for the two different SciFi cables at a signal level of 400 mV. The graph shows the percentage of pre-emphasis of the signal level on the horizontal axis and the corresponding parameter values on the vertical axis.

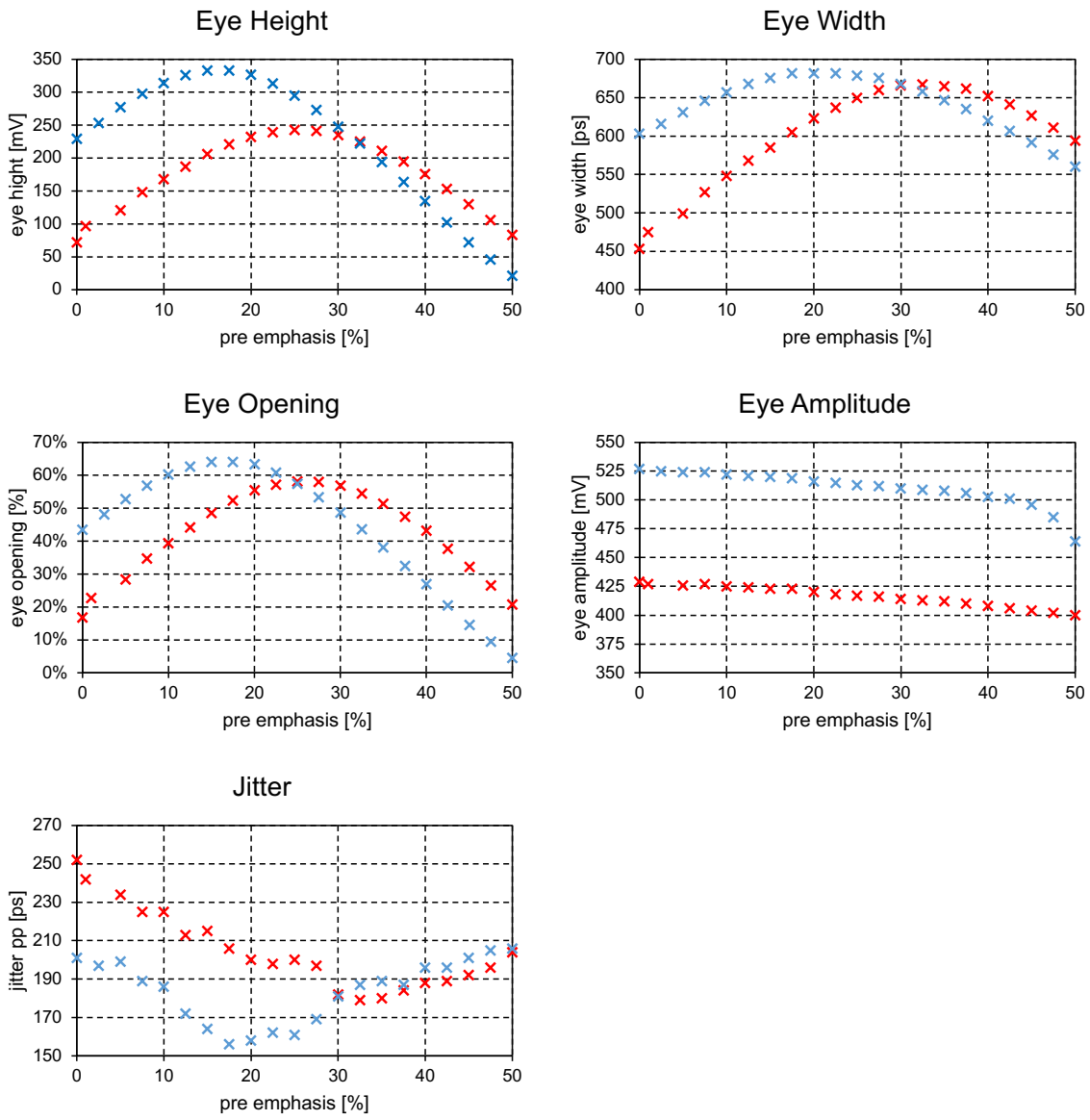

Figure 3.21: The different values of the eye diagrams on the y-axis for different pre-emphasis settings in percent of the signal level, which was selected as 400 mV.
In red are the values for the micro-twisted pair cable made of raw cable from the Mu3e coil (lower impedance), and in blue are the values for the micro-twisted pair cable made of raw cable from the CMS coil (high impedance).
It can be seen that the cable with lower impedance, especially with less pre-emphasis, has a significantly smaller eye-opening, but with a sufficiently large pre-emphasis, the eye-opening can be significantly enlarged.

Despite the slightly different measurement setup, the measurements of Figure 3.21 are

practically identical in all values to the measurements of the prototypes of the vertex cable (Figure 3.18). This suggests that the measurement process was accurate and reliable and that the two cables have similar properties.
Above all this measurement supports the result that communication is possible via the cables with sufficient pre-emphasis.
However, further testing may be necessary to fully understand any differences or similarities between these cables regarding their performance and functionality.

3.7 Differences in the Cable Size

As shown in the measurements, there seems to be a difference between the cable on the new Mu3e coil and the cable on the old CMS coil. Especially the impedance of the two cables is clearly different.
The impedance of a differential pair of cables is determined by the two values of the diameter of the cables and the distance between the two cables[49].
These two values should, therefore, be measured in this section for the cables from both coils.

To investigate a potential cause for the varying cable performance, both cables undergo measurement using a digital microscope at the PSI. Section 3.1.1 outlines the projected sizes upon which the cables were ordered from the company.
The cables at the PSI are being cut open with extreme care using a very fine knife. Once opened, they are placed upright on a surface, and a microscope is pointed directly at the interface. This allows for the sizes of the individual components of the cable to be measured using the microscope's scale function.
The results illustrated in Figure 3.22 demonstrate that the distance between the raw cable pairs originating from the CMS Coil, which is expected to comprise twice the 0.025 mm polyamide isolation and once the 0.010 mm aromatic polyamide region, is measured to be 0.097(10) mm, a value significantly greater than the anticipated 0.060 mm. Conversely, the distance between the raw cable pair derived from the Mu3e coil is measured to be 0.067(7) mm, which is much closer to the anticipated value of 0.060 mm.
These findings suggest a discrepancy between the expected and actual values.
The remaining measured values all seem to agree with the expected order values, see section 3.1.1.
It can, therefore, be assumed that the cable, which is incorrectly produced, was the CMS one. However, as the cable fitted exactly to the requirements of the CMS experiment, this was not remeasured and checked in the past.

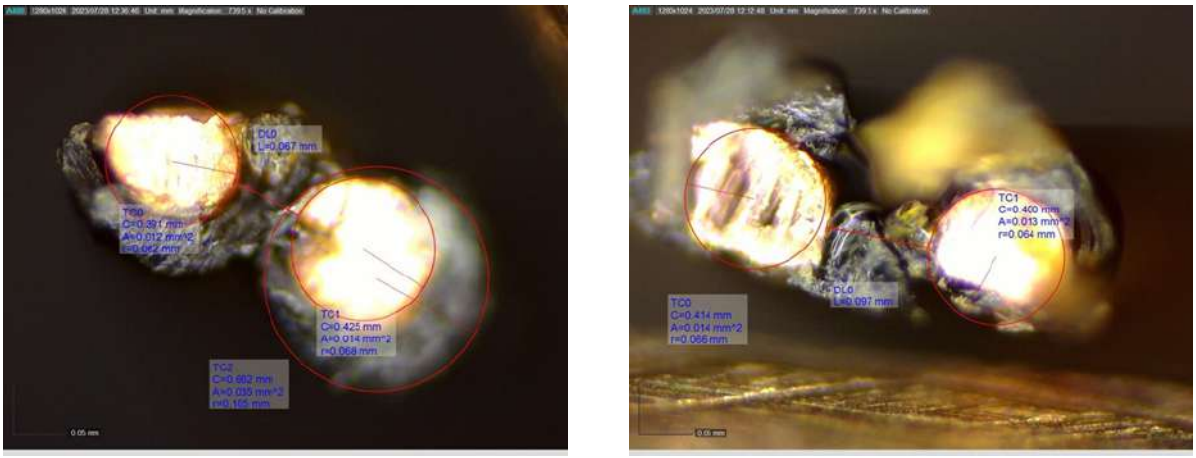

(a) Mu3e Spool (b) CMS Spool

Figure 3.22: The measurement of the cable cross-section on a digital microscope for different micro-twisted pair bundles from different coils.
It can be seen that the distance between the two cable pairs of 0.097(10) mm measured for the CMS coil is too large compared with the expected value from the order, and differs from the 0.067(7) mm measured for the Mu3e coil. Based on the datasheet, when ordering the cable, one would expect a cable thickness of 0.060 mm.
The other measurements seem to agree with the order.

It is important to remember that measuring a cable's cross-sectional area may not always be accurate due to the distortion caused by cutting a thin wire. For obtaining a more precise measurement, it is recommended to cast the cables with epoxy resin before cutting a cross-section with a fine grinding machine. Unfortunately, machines and equipment for such a measurement are not available at PSI.
An error of 10% was assumed for all measurements with the microscope.

3.8 Quality Control (QC) test

A QC test was designed to test the future cables that will be manufactured for the detectors. This is based on the properties of the cables that were measured here and on the fact that the measurement of the eye diagrams and the BER have shown that communication with the cables is possible.

The measurements of the BER and the eye diagrams are too time-consuming to set up and carry out and are therefore, not measurements for a QC test.
The QC test should be limited to the measurement of impedance, insertion loss and crosstalk. The advantage of these measurements is that they can all be carried out with one VNA, which saves a lot of time. Previous measurements for Vertex cables with 4 DAB-STP adapters or SciFi cables required approximately 3 hours of measurement time for all 3 measurements.
In addition to the three measurements mentioned above, the QC test should also include a connection measurement.

The four measurements for a complete QC test are as follows:

Connections: The first step is to check the connections of the cables to check that there is no short circuit anywhere. To do this, the cable is connected to the diagnostics board, and a voltmeter is used to check on the board whether any wires are connected. This would be equivalent to a short circuit in the cable or on its boards and would immediately render the cable unusable.

Impedance: The impedance for all measurements should not be less than $70\,\Omega$ on average over the entire measuring length of 1 m, at such a low impedance, it has not yet been possible to test transmission. According to the standard deviation, significantly more than 99.99% of all measurement data should be above this. It is also important to ensure that there are no individual peaks where the impedance suddenly exceeds $110\,\Omega$ or more, as this would indicate damage to the cable.

Insertion loss: For the insertion loss, it has been shown that the value at the fundamental frequency of 625 MHz is particularly suitable for comparison. There, the insertion loss must not be less than $4.75\,\mathrm{dBm}^{-1}$ for the vertex cables and $6.5\,\mathrm{dBm}^{-1}$. This is because, according to previous measurements, it is not certain that the signal quality is guaranteed below these values.
$4.75\,\mathrm{dBm}^{-1}$ already means a signal loss of over 40% of the input signal. Even larger numbers would mean that at frequencies of over 1 GHz, the signals with possibly less than 10% have a size that may no longer be distinguishable from the noise.
Furthermore, a brief visual observation of the insertion loss across all frequencies should

show that the insertion loss increases exponentially with the increase in frequency and that there are no unexpected peaks or frequencies that are particularly strongly attenuated.

Crosstalk: The crosstalk should not exceed 2% on average for any wire; this could then become a variable that influences the signal quality meaningfully.

If individual values are not fulfilled for individual differential signal cables, this does not mean that signal transmission is not possible, but only that this cannot be confirmed by current measurements. For these cables, a further measurement of signal quality, such as the BER, would then be appropriate.

The measurement is very time-consuming for all cables.
To save some time, it should be sufficient to carry out the exact detailed measurement for only one cable of a delivery.
For the other cables, it should also be sufficient to carry out an abbreviated measurement consisting only of connection and impedance measurements. These two measurements should reveal all possible connection faults and also the vast majority of gross cable faults.

The target values are a suggestion based on the measurements and can also be changed in the future with more data available.

Chapter 4

Transmission quality of a MuPix Ladder

In this chapter, the signal transmission from the ladder to the DAQ system will be tested and some DAC values will be found on the sensor at which the signal transmission is optimized.
This is an important point, as measurements on the micro-twisted pair cable have already shown that a careful selection of the transmission settings, especially the pre-emphasis, will be necessary for error-free data transmission.

For this, a setup that represents a simplified version of the envisaged experimental setup, with only a single ladder and a single front-end board was utilized.

This setup will then be used to measure the transmission quality by measuring the eye diagrams of the transmitted signal with a SDA, as in chapter 3, where eye diagrams have already been used. The eye diagrams, in particular the value of the opening of the eye diagram, can then be compared for different setting values, from which an optimum value can be found.

4.1 Measurement Setup

For a successful measurement, it has been specified that specific instruments and a data acquisition system are required to accurately read out the Mupix Ladder on the DAQ PC. This system involves a single ladder and a front-end board. The structure of the setup is similar to what will be used in the Mu3e experiment. The following reference is recommended for further information: [50].

MuPix Ladder:
In this experiment, a downstream ladder is being measured. The ladder is a series of six sensors that are all connected to an HDI circuit board. This ladder is being placed firmly on an assembly tool, which is also planned to be used in the Mu3e experiment. This tool is designed to attach the endpiece flex with an interposer to the ladder using a screw connection. The ladder shown in Figure 4.1 is resting on the assembly tool, with the endpiece flex visible.
The ladder must be kept cool, for this, it is placed in a Memmert CTC 256 cooling chamber. This cooling chamber can lower the temperature to -40 degrees Celsius and regulate humidity to 10% at temperatures as low as 10 degrees Celsius, with the aid of external compressed air. The cooling chamber is controlled by a separate Computer. On this computer, the temperature and humidity can also be monitored via additional sensors indoors.

Power Supply:
To power the ladder, it is connected to a high-current source and a low-current source, as explained in section 2.4.1. The high-current source is a Keithley 2450 SourceMeter, and the low-current source is a Rohde & Schwarz HMP 4040.
In order to be able to select the voltage directly at the ladder of the low current source more precisely, a sensing cable is used, which serves as a voltage reference directly at the ladder.
Unlike a micro-twisted pair cable, the sensing cable contains two sets of two twisted pair wires.
Both current sources are connected to the DAQ PC, so it is later possible to control the voltage directly over the DAQ PC.

The MuPix Ladder is connected to the DAB via the Endpiece Flex and a micro-twisted pair cable. The DAB is connected directly to the FEB and is able to apply an equalizer and/or pre-emphasis to the signal over a chip.
Since only one ladder is being used in this experiment, only one DAB-STP connection of the cable is in operation.

Data Acquisition System (DAQ):
The custom-developed FEB is part of the DAQ, which also consists of a switching board and an Field Programmable Gate Array (FPGA) PC. The DAQ is responsible for multiple tasks, such as registering and aligning data in real time, as well as analyzing it.
The data process is as follows:
The FEB sorts the received hits in time and then forwards the data to the switching board via optical cables. The switching board synchronizes the incoming data streams from the front-end boards and times the different data streams. In this setup, just one FEB is connected.
After this, the data is sent to a Terasic DE5a-Net-DDR4 board, which is placed inside a

PC with a Graphics Processing Unit (GPU). This board has an ARRIA10 FPGA and DDR4 RAM. The Mu3e experiment will use later the FPGA together with the GPU to perform event reconstruction while the data is cached in the DDR4 RAM[13].
In the FPGA board, a clock with a frequency of 125 MHz is also generated to synchronize various data streams and enable data synchronization. The clock signal is then transmitted to the ladder through the FEB.
To ensure that the clock signal is transmitted accurately, the FEB applies pre-emphasis to amplify it before transmitting it via the micro-twisted pair cable. This amplification compensates for any insertion loss that may occur during transmission, ensuring that the clock signal is received accurately at the other end.

Maximum Integration Data Acquisition System (MIDAS):
Once the DAQ has collected the necessary data, it is securely transferred to the MIDAS system. MIDAS is a widely used software application that enables real-time data acquisition, storage, and analysis across a range of experiments.
One of the features of MIDAS is its interface, which allows for in-depth analysis of the collected data.
Of particular interest for this task is the integrated slow control system, which enables, in this case, the control of the two power supplies connected to the computer via an Ethernet connection.
The Slow Control system also offers the capability to configure the sensor over the DAC, including the flexibility to adjust parameters like the threshold level. Additionally, it allows for the fine-tuning of values like the signal level or the pre-emphasis of the outgoing detector signal, which are especially relevant for this task.

Serial Data Analyzer (SDA): The output diagrams are measured using a tool called the SDA (like in chapter 3). The differential voltages directly on the DAB are measured before the equalizer/pre-emphasis chip. The SDA used is the LeCroy SDA 6020.
The eye diagrams are evaluated by the SDA by the parameters eye-opening, eye amplitude, eye height, eye width, and Q-factor.
The first four have already been described in chapter 3. New in this chapter is the Q-factor, which is a value for the signal transmission quality. The Q-factor is calculated as the eye-opening's width divided by the noise's standard deviation. The higher the Q-factor, the better the signal is separated from the noise.

Figure 4.1 shows the ladder together with the Endpiece Flex placed in the climate chamber, and figures 4.2 and 4.3 show the experimental setup as described outside the climate chamber.

Since this setup is a scaled-down version of the actual Mu3e experiment, this setup offers the possibility to measure much more than just the data transmission quality in the future.

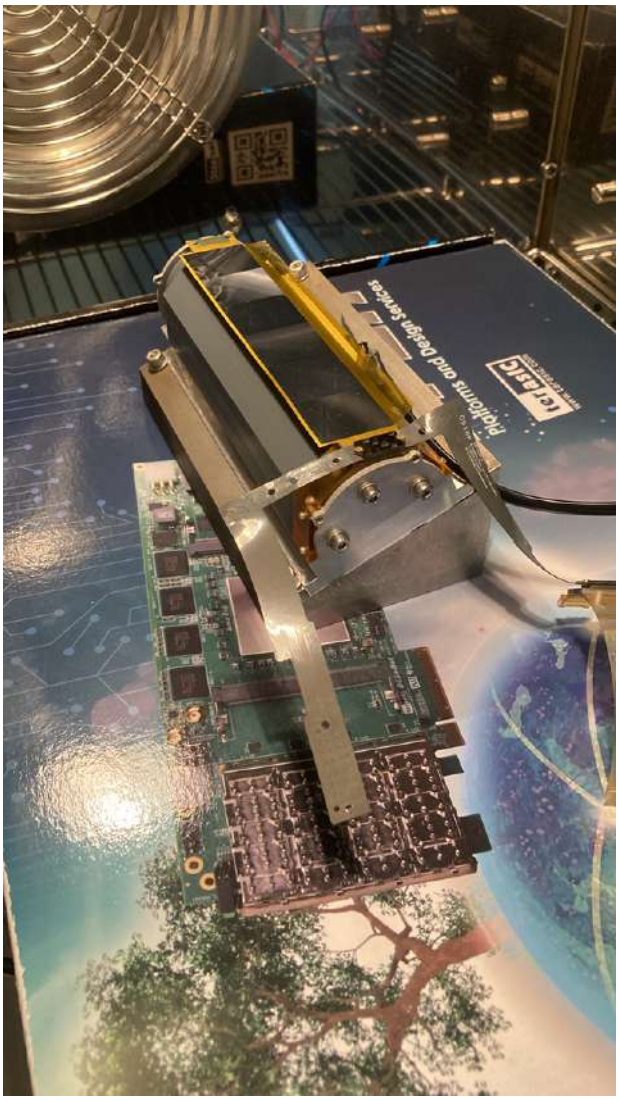

Figure 4.1: The ladder is screwed on the assembly tool and directly connected to the Endpiece Flex in the Climate Chamber.

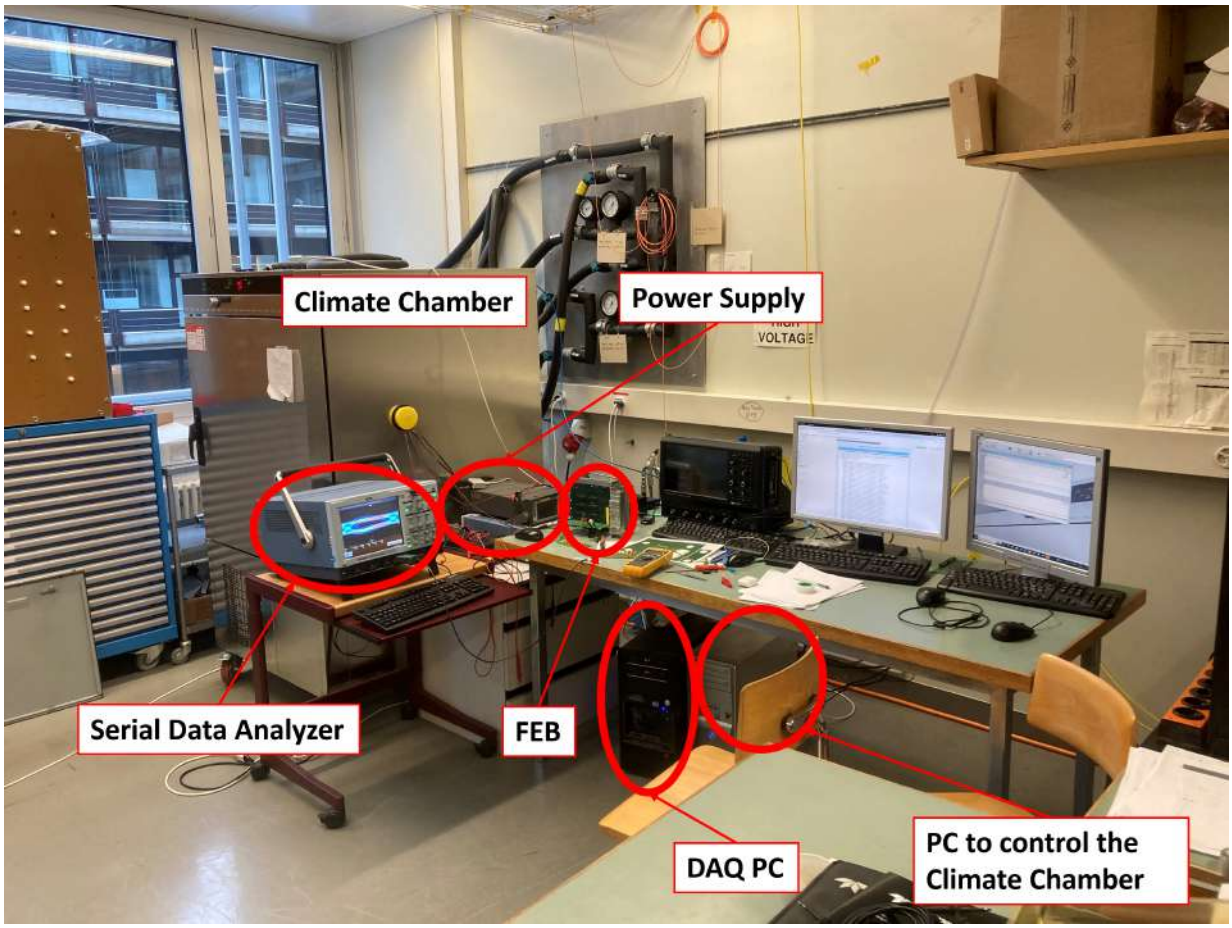

Figure 4.2: An overview of the experimental setup to characterize the Mu3e ladder.

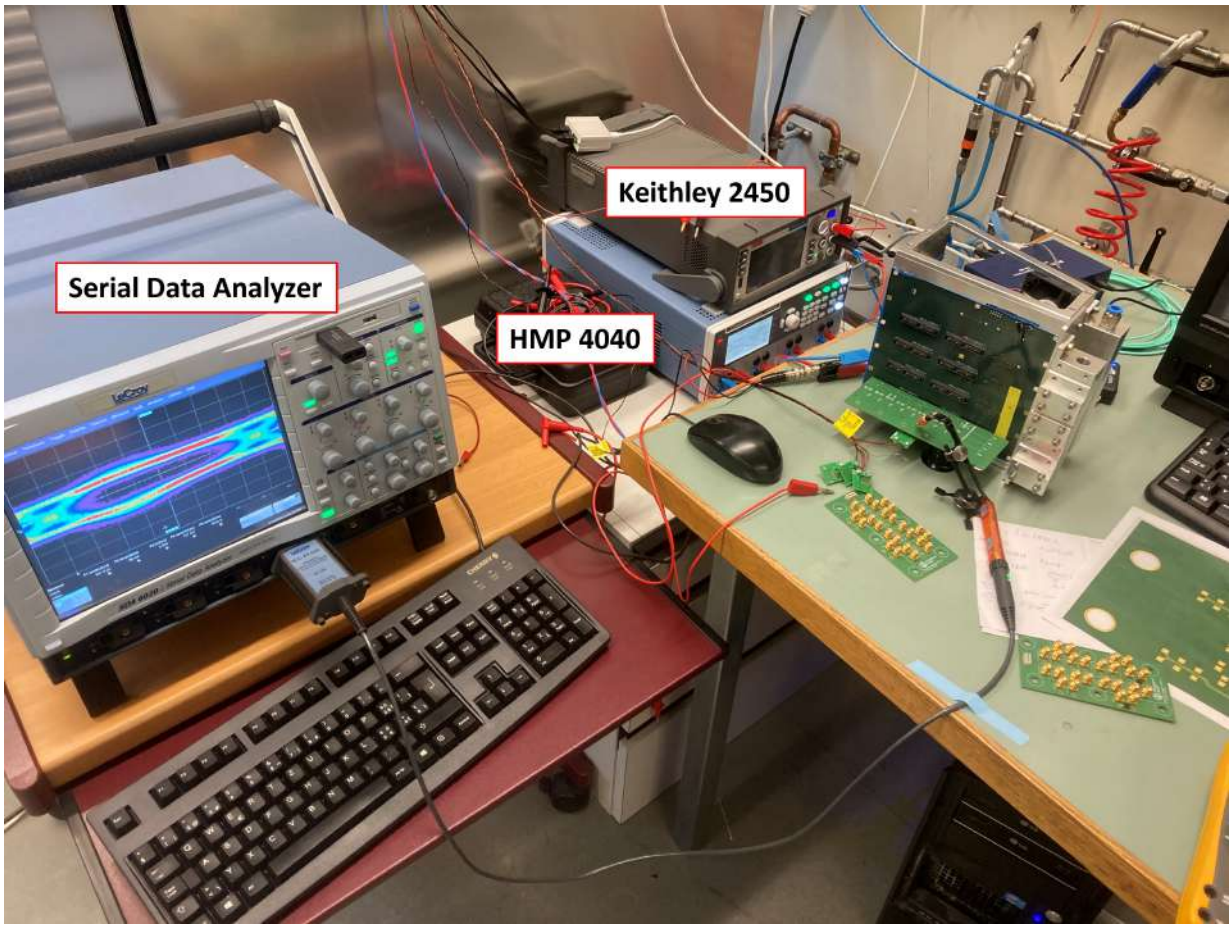

Figure 4.3: The experimental setup for measuring Eye Diagrams on the SDA and the two Power Supplies used in this Setup.

4.2 Measurement

To measure the data transmission quality with different settings, various DAC values are available in the Clocking&Data Sensor Settings. These DAC values can be configured to various values in the MIDAS slow control system. Table 4.1 shows these.

Variable	**Description**
VNTimerDel	Bias for delay cell/Power Switch
VPTimerDel	Ro-buffer delay cell
VNDAC	Reference voltage for tuning
VPFoll	AmpOut test output control for the CSA
VNComp	Current Source for comparator
VNHB	Hitbus test output control
VNComp2	Current Source for comparator
VPPump	Reg Speed of PLL
VNDcl	Current Source Dcl logic
VPDcl	Current Source Dcl logic
VNDelPreEmp	Delay of pre-emphasis Signal
VPDelPreEmp	Delay of pre-emphasis Signal
VNDelDcl	Delay for Differential current line (Dcl) clock
VPDelDcl	Delay for Dcl clock
VNVCO	Control Voltage Voltage-controlled oscillator (VCO) of the PLL
VPVCO	Control Voltage VCO of the PLL
VNLVDS	Output Amplitude Low-Voltage Differential Signaling (LVDS)
VNLVDSDel	Output Amplitude LVDS Pre-emphasis

Table 4.1: The Clocking&Data DAC settings for the MuPix sensor as described in the documentation[20] and [51].

For this thesis, the signal quality by changing the parameters of VNLVDS, VNLVDSdel, VNDcl, and VPDcl is measured, as these seem to be the parameters most directly related to the signal quality.
VNLVDS and VNLVDSdel are the parameters that represent the signal amplitude and the pre-emphasis of the Signals. Measurements of micro-twisted pair cables have already shown (chapter 3) that the transmission quality of these cables is highly dependent on the level of pre-emphasis and the signal amplitude.
VNDcl and VPDcl are parameters that determine the global level of the current of the Differential current line (Dcl). As these values directly influence the transmission, it is obvious that this directly influences the transmission quality.
In order to analyze the direct correlations between VNLVDS with VNLVDSdel and VNDcl with VPDcl, these two values were each measured together. For time reasons, all 4 values were not measured together.

Since other parameters can also significantly change the values, it would certainly be recommended to measure other parameters in the future in order to test whether they have a major influence on the signal quality.

Measurement procedure
The general procedure for measuring the values was as follows:
The ladder to be measured was cooled at a constant temperature of 10 degrees Celsius and a constant humidity of 10%.
Since it was determined by analyzing the BER over MIDAS that the transmission via link 10 (chip 1 data B) is the most stable, the voltage was measured with the SDA directly on this link on the DAB and this before the equalizer/pre-emphasis chip on the DAB. This is because the signal was subsequently heavily disturbed in the form Figure 5.2 shows a comparison.
It is still unclear why this link is the most stable, but the cable is unlikely to be the cause. Measurements on the cable did not reveal any significant differences between the individual sub-cables.

All other variables, see Table 4.1, apart from the two that were measured, were set to a fixed value when configuring the sensor.
The two values to be measured are varied between a selected minimum and maximum value, with a chosen steps size.
The eye diagrams are then measured for about 10 seconds using the SDA for each choice of these values. After about 10 seconds, the eye diagrams are saved, with the SDA. The SDA directly evaluates some parameters, such as eye-opening.

Furthermore, the current consumption of the low-voltage power supply was also measured. For this, the same parameters were again varied in pairs, and the sensor was reconfigured. Each time, the current consumption of the low-voltage source was then measured using MIDAS slow control. The voltage was kept constant over the entire time. The remaining values are again set to a fixed value.

4.3 Result

VNLVDS and VNLVDSdel

The eye diagrams were measured for ladder 463-00003-000002 for all even values of VNLVDS and VNLVDSdel between 0 and 62 (including 0). The remaining variables were selected as shown in Table 4.2.
The measured data of the eye-opening factor and the Q-factor of the eye diagrams are presented in scatter and contour plots in Figure 4.4. The maximum value is marked on the scatter plot, and contour lines are shown at 10%, 25%, 50%, 75%, and 95% of the maximum value.

In order to compare the values of the measurements between two different ladders, a second measurement was also carried out on both ladders 0463-00003-000002 and 0450-0001-0000001, whereby odd values of VNLVDS between 25 and 35 and odd values of VNLVDSdel between 5 and 15 were selected. The remaining variables were again selected as shown in Table 4.2.
Figure 4.4 shows the measurement of the eye-opening factor of the eye diagram measurement for the two ladders.

Figure 4.5 shows the measurement for the current consumption at the low current source of ladder 0463-00003-000002 for all values of VNLVDS and VNLVDSdel between 0 and 63. The remaining variables were again selected as shown in Table 4.2.

Variable	Value
VNTimerDel	20
VPTimerDel	6
VNDAC	0
VPFoll	0
VNComp	0
VNHB	0
VNComp2	5
VPPump	30
VNDcl	20
VPDcl	36
VNDelPreEmp	16
VPDelPreEmp	16
VNDelDcl	32
VPDelDcl	32
VN CO	23
VPVCO	22

Table 4.2: The DAC values, which were chosen to measure eye diagrams and power consumption for different VNLVDS and VNLVDSdel values.

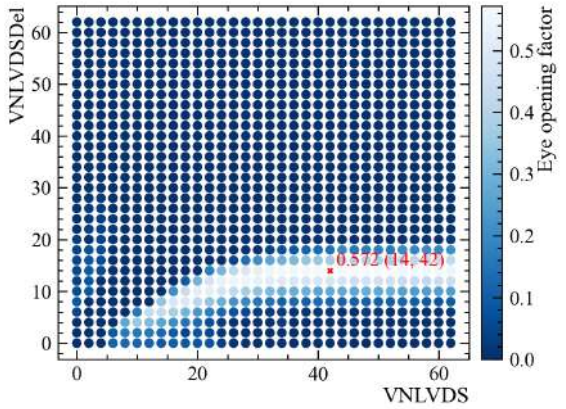

(a) Scatter Plot - eye-opening factor

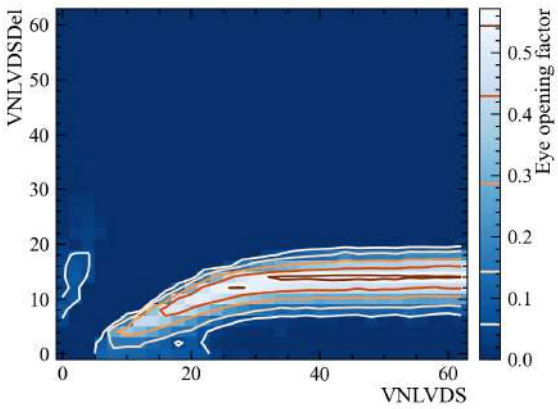

(b) Contour Plot - eye-opening factor

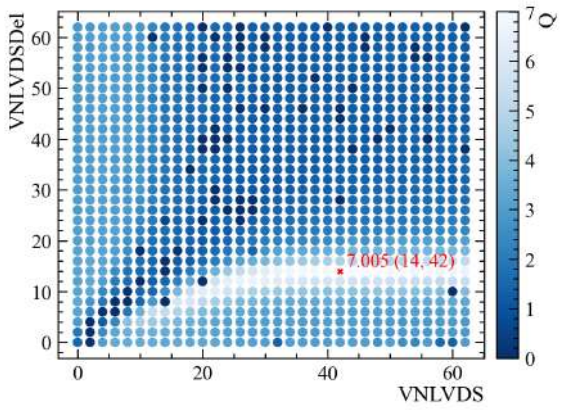

(c) Scatter Plot - Q-factor

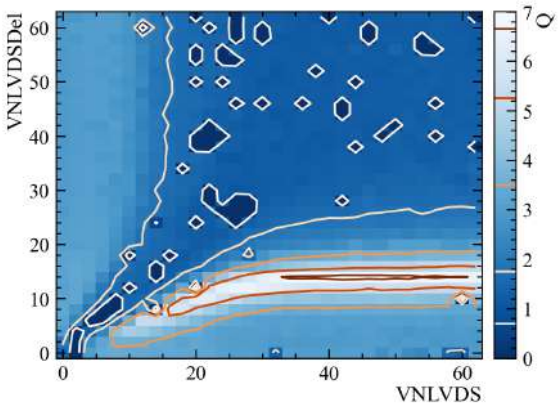

(d) Contour Plot - Q-factor

Figure 4.4: The values of the eye-diagram were measured for varying VNLVDS and VNLVDSdel, both for all even values between 0 and 62 (inclusive 0), while keeping other values constant at values shown in table 4.2.
In the scatter plot, the largest value is highlighted in red. The contour plot shows lines at 10%, 25%, 50%, 75%, and 95% of the maximum value.

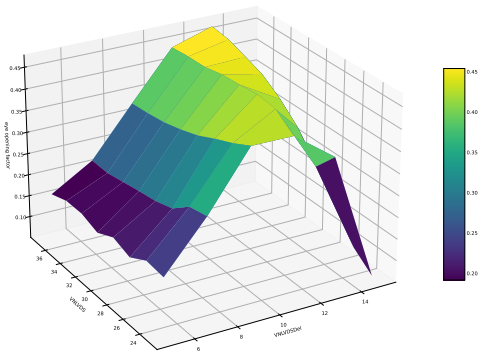

(e) 0463-00003-000001 - eye-opening factor

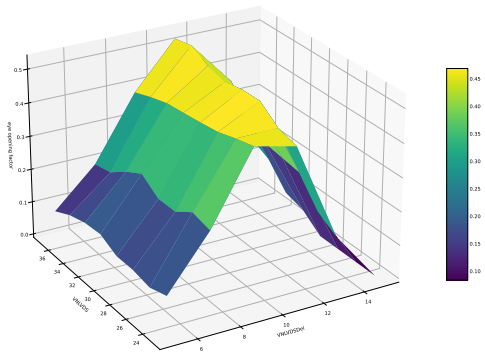

(f) 0463-00003-000002 - eye-opening factor

Figure 4.4: The values of the eye-diagram were measured for varying VNLVDS for all odd values between 25 and 35 and VNLVDSdel for all odd values between 5 and 15 while keeping other values constant at values shown in Table 4.2.
The height of the plot and the color marks the respective value measured on the eye diagram.

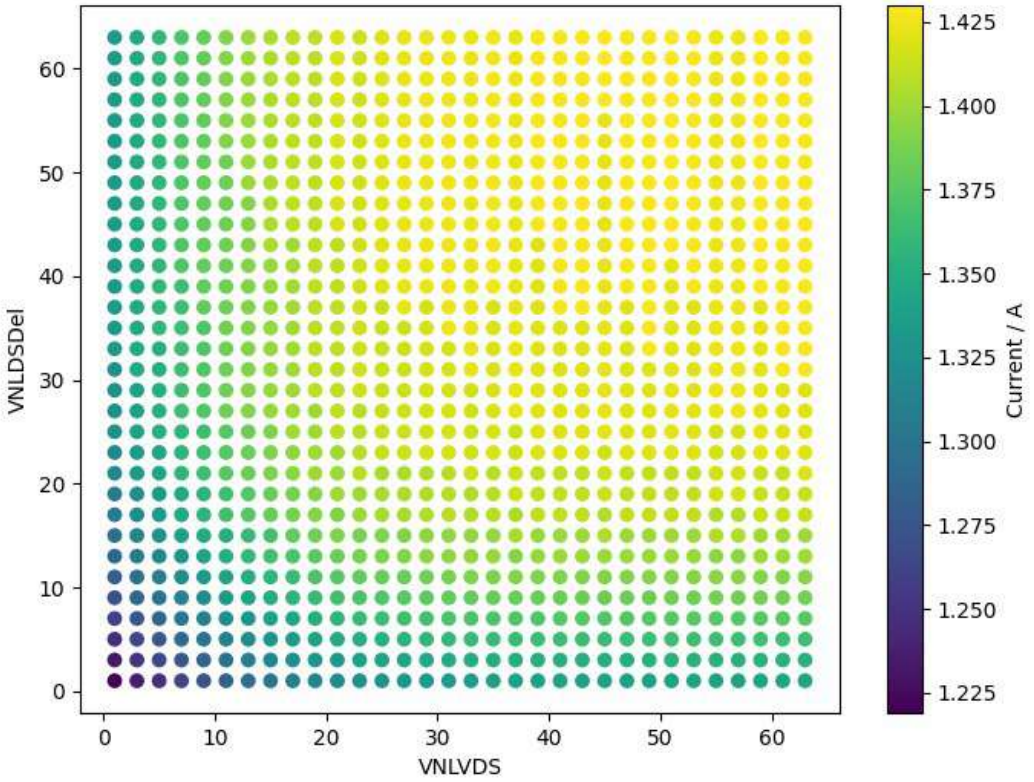

Figure 4.5: The current in amperes at different values of VNLVDS and VNLVVDSdel, while other values are kept constant, at values shown in Table 4.2.

The results show that optimizing the eye amplitude in these two parameters for ladder 0463-00003-000002 without making any big compromises is possible. The eye-opening factor and the Q-factor have both reached their optimal value when the value of VNLVDSdel is 14 and VNLVDS is 42, which means that the largest eye-opening and the clearest eye are present at one value.

The available bandwidth for selecting good working values is significantly larger for VNLVDS than for VNLVDSdel. Even small deviations of 4 points from the optimum value can cause significant changes in the eye-opening and eye quality (Q-factor). However, small deviations from the optimal value are not a big problem for VNLVDS as there are many other similar optimal values around it due to the barely changing amplitude on high values.

When it comes to power consumption, the measurement shows, that increasing the signal amplitude results obviously in higher power consumption at higher VNLVDS values, up to a maximum. The same applies to VNLVDSdel values. This was expected because a pre-emphasis causes an increase in the signal's voltage when changing bits, resulting in

higher power consumption.

It is visible in Figure 4.4 that there is a linear relationship between VNLVDS and VNLVDSdel in the measurement of the eye-opening factor. However, this linear relationship only applies to VNLVDS values up to 32. Beyond that point, there is no dependency, and values remain constant. This observation is also valid for the Q-factor and power consumption, which all become constant beyond VNLVDS values of 32. This suggests that there is a maximum output amplitude or an extremely weak dependence of the amplitude on VNLVDS values beyond 32.

Based on the acquired data shown in Figure 4.4, it is evident that a noticeable disparity exists between the two ladders measured.
The largest eye-opening of ladder 0463-00003-000001 is smaller than that of ladder 0463-00003-000002 but also with a smaller value of VNLVDSdel.
This could indicate differences between the sensors. If this proves to be the case, it would mean that each ladder would have to be optimized independently for the values of VNLVDS and VNLVDSdel.
However, measurements on other ladders would be necessary to investigate this. Because the significance of the measurement of ladder 0463-00003-000001 is not very strong as the ladder is damaged. Some sensors were loose and have come off, and the strong fan in the climate chamber has caused the bending to increase to a kink. However, the extent to which this damage affects the performance of the other sensors is unknown.

VNDcl and VPDcl

The eye diagrams were measured for ladder 463-00003-000002 for all even values of VNDcl between 2 and 52 and all even values of VPDcl between 2 and 62. The remaining variables were selected as in table 4.3.
The measured data of the eye-opening factor and the Q-factor of the eye diagrams are presented in scatter and contour plots in Figure 4.4. The maximum value is marked on the scatter plot, and contour lines are shown at 10%, 25%, 50%, 75%, and 95% of the maximum value.

Figure 4.7 shows the measurement for the current consumption at the low current source of ladder 0463-00003-000002 for all values of VNLVDS and VNLVDSdel between 0 and 63. The remaining variables were again selected as shown in Table 4.3.

Variable	Value
VNTimerDel	20
VPTimerDel	6
VNDAC	0
VPFoll	0
VNComp	0
VNHB	0
VNComp2	5
VPPump	30
VNLVDS	42
VNLVDSdel	14
VNDelPreEmp	16
VPDelPreEmp	16
NDelDcl	32
VPDelDcl	32
VNVCO	23
VPVCO	22

Table 4.3: The DAC values, which were chosen to measure eye diagrams and power consumption for different VNDcl and VPDcl values.

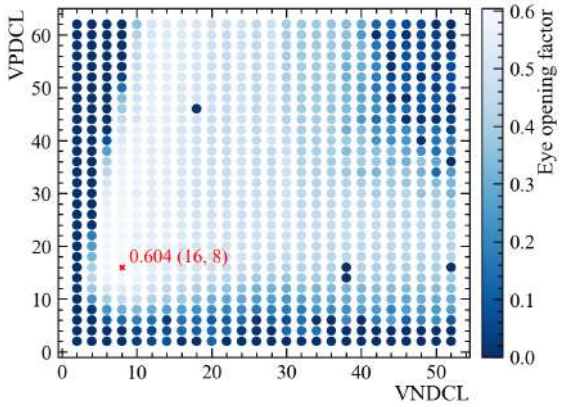

(a) Scatter Plot - eye-opening factor

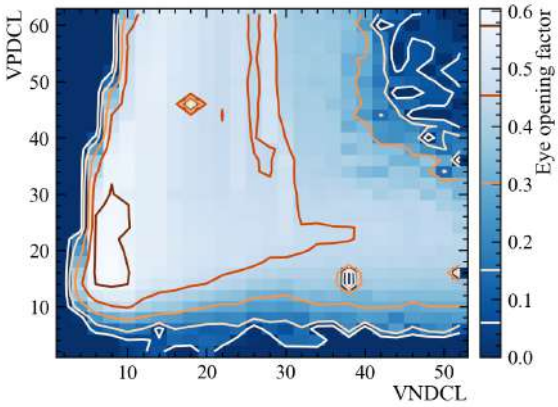

(b) Contour Plot - eye-opening factor

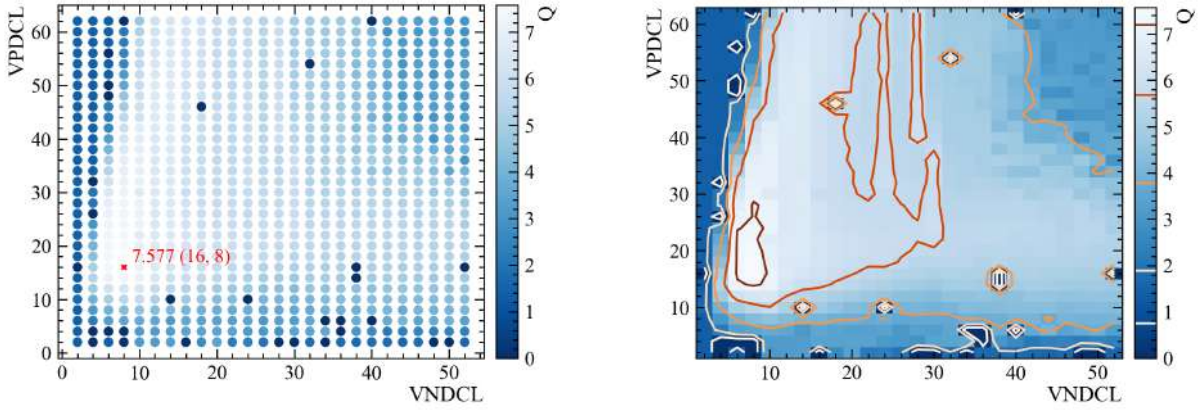

(c) Scatter Plot - Q-factor

(d) Contour Plot - Q-factor

Figure 4.6: The values of the eye-diagram were measured for varying VNDcl and VPDcl, both for all even values between 0 and 62 (inclusive 0) while keeping other values constant at values shown in table 4.2.
In the scatter plot, the largest value is highlighted in red. The contour plot shows lines at 10%, 25%, 50%, 75%, and 95% of the maximum value.

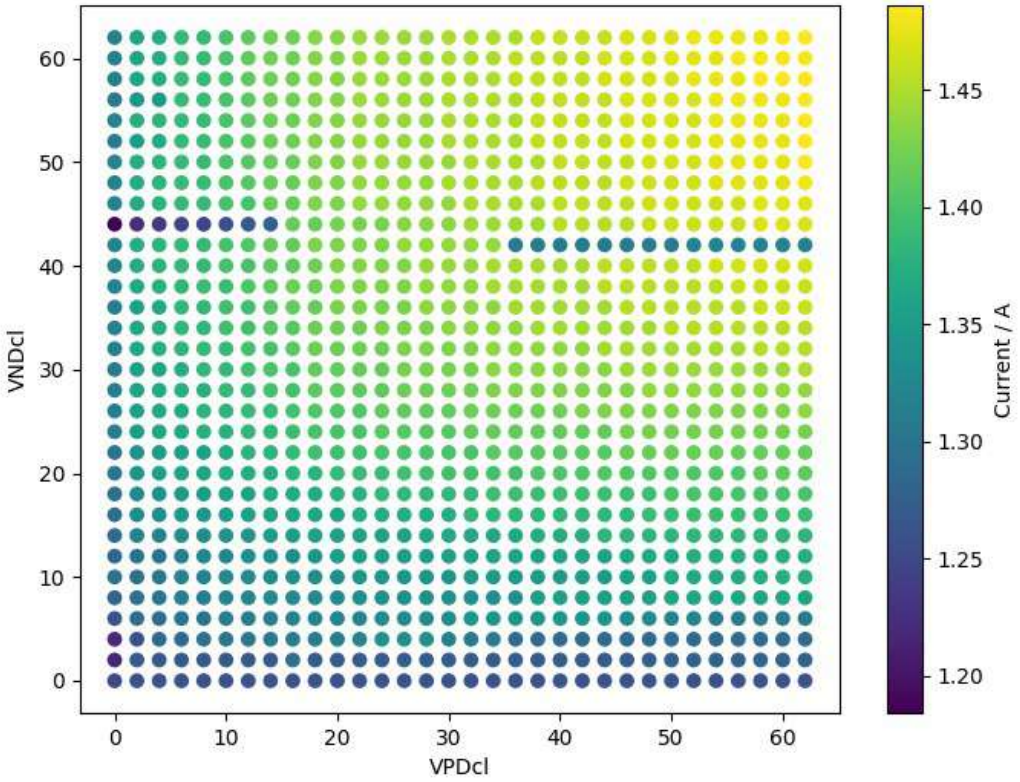

Figure 4.7: The current in amperes at different values of VNDcl and VPDcl, while other values are kept constant, at values shown in table 4.2.

It is apparent from the analysis that the maximum values for both the eye-opening factor and the Q-factor occur at the same DAC value (VNDcl has a value of 8 and VPCL has a value of 16). Upon examining the scatter plot, it can be inferred that these DAC values generally benefit from having VPDcl equal to twice the value of VNDcl. This observation also holds true for eye height and eye width, as can be seen in the appendix.
By using these DAC values, a high degree of eye amplitude (eye-opening factor) can be achieved while keeping the noise level (Q-factor) to a minimum.

Points with higher VNDcl and VPDcl have a slightly smaller eye, but are more stable against deviations in the values of VNDcl and VPDcl. This could be advantageous for the experiment.

As expected, the current in the cables, which depends on the two variables, is directly related to the current consumption of the sensor readout and transmission electronics, as Figure 4.7 shows.

Chapter 5

Conclusion & Outlook

Characterization of the micro-twisted pair cables

Based on the measurements taken, it was observed that the impedance and insertion loss of the two prototype cables made of wires from the new Mu3e coil remained relatively consistent overall measurements. However, the crosstalk values varied due to the physical proximity of the cable pairs.
After conducting measurements of the bit error rate and eye diagram, it was determined that error-free communication through the cable is achievable by adjusting the pre-emphasis or the equalizer. This is the basic criterion required to use the cable in the Mu3e experiment as intended.
However, the difference between the wires used in the CMS experiment and the newly ordered wires is concerning, as the company could not name any difference between the cables on demand.

In the context of an experiment, it is essential to evaluate the suitability of future manufactured cables that are intended for use. However, performing a comprehensive test of all data cables to determine their bit error rate and eye diagrams is not always feasible due to the time constraints involved. In such cases, measuring the impedance, insertion loss, and crosstalk of the cables is more practical and requires less time and effort.
It is worth noting that while these measurements do not directly indicate the signal quality, we can compare them with the measurements of the two prototype cables, from which benchmark values can be found. This QC test then provides a good prediction of the functionality of the cables.
If this is still too time-consuming, a shortened test, as suggested, is also possible.

In conclusion, it can be stated that the cables are well understood. Thus, further resources can be directed towards other experiment aspects that require more attention.

Transmission quality of a MuPix Ladder

It has been demonstrated that communication with the planned setup is possible in principle. However, it is important to note that the quality of communication largely depends on the selected DAC values. Specifically, VNLVDS and VNLVDSdel values have a significant impact on the eye-opening factor. Even minor deviations from the optimal DAC values in these parameters could change the eye-opening factor significantly.
The eye-opening factor for changes of VNDcl or VPDcl is much more stable with variations of the DAC values around the optimum point.
This highlights the criticality of carefully selecting VNLVDS and VNLVDSdel values for each sensor.

The measurements have so far always been taken on link 10 because this is one of the best connections. Other connections apart from link 11 do not provide comparably stable connections. The reason for this has not yet been clarified, but as the cable connections are already measured in chapter 3, this factor can be ruled out. However, this is something that should definitely be investigated in further measurements, as a stable connection for all links is essential for the experiment.
It has been demonstrated that despite being one of the most stable connections in two of the ladders tested, link 10 still experienced numerous bit errors. Figure 5.1 presents the bit error rate for two ladders over several hours. It is evident that stable, error-free communication over such an extended period is not yet feasible. However, this situation could potentially improve with better sensor settings.

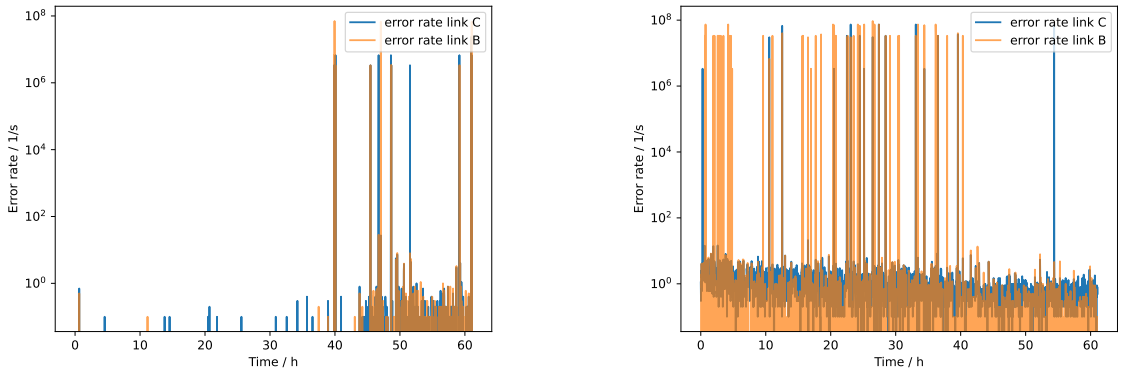

(a) Ladder 0463-00003-000002

(b) Ladder 0463-00003-000001

Figure 5.1: During signal transmission through the ladder, the bit error rate was measured with VNLVDS values of 29 and VNLVDSdel values of 12, with the remaining values as shown in Table 1.
The links shown here are Link C (link 10 on the DAB) and Link B (Link 11 on the DAB), as these two are by far the most stable in transmission.

It is advisable to perform additional measurements on more DAC values shown in Table 4.1 to be able to optimize more values during data transmission. Furthermore, it would be interesting not only to measure two values together but to extend the measurement to 3 or 4 variables together in order to find more dependencies on each other. These additional measurements could be expected to further improve the data transmission rate.

Something else that should be checked is the behavior of the equalizer/pre-emphasis chip on the DAB. In the case of this measurement, both were switched off in the chip, but the chip still works as an amplifier.
The measurements were all taken before the chip on link 10, but it would also be interesting to take them directly after the chip. However, all previous measurements show a faulty signal after the chip. See an example of the same signal in Figure 5.2 before and after the chip. It is assumed that the issue being experienced may have been caused by improper termination of the signal at the front-end board with the incorrect impedance. However, further investigation is needed to confirm this hypothesis and fully understand the root cause.

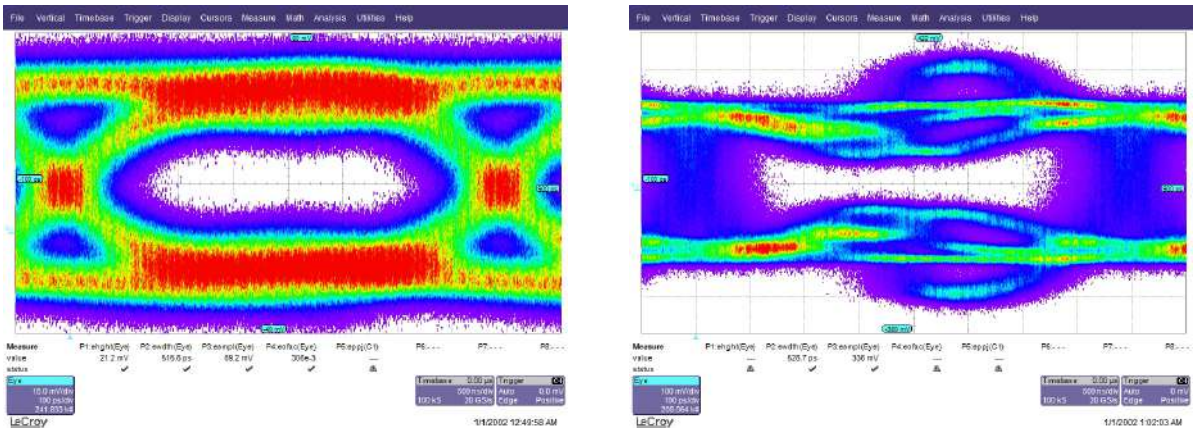

(a) Before the chip (b) After the chip

Figure 5.2: The display of the same signal with sensor settings as in table 1, once before the switched-on equalizer/pre-emphasis chip on the DAB and once after. Both on link 10.

To conclude, it can be asserted that the measurements on the ladder have yielded preliminary outcomes. Nevertheless, additional measurements are imperative for future analysis.

Chapter 6

Appendix

In this section 6.1 and 6.2, more figures for different parameters of the evaluated eye diagrams are shown, which were evaluated in chapter 4.

6.1 Measurement of VNLVDS and VNLVDSdel

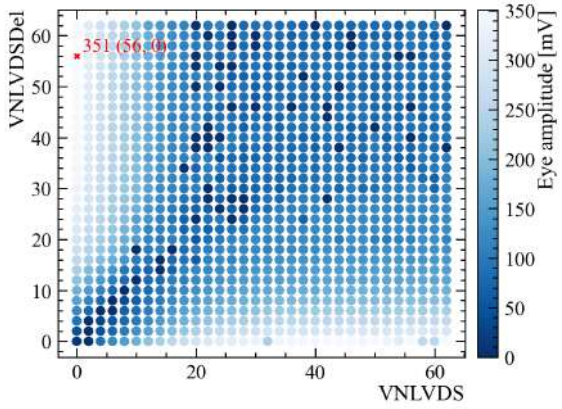

(a) Scatter Plot - eye amplitude

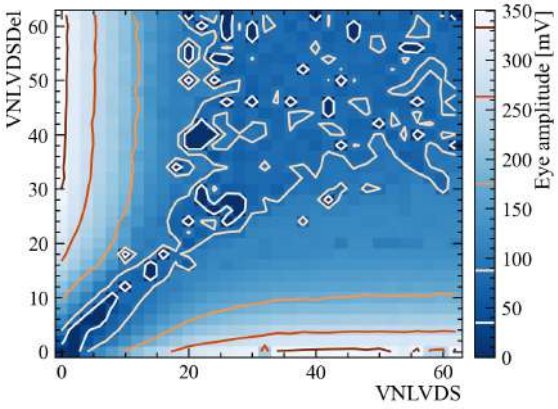

(b) Contour Plot - eye amplitude

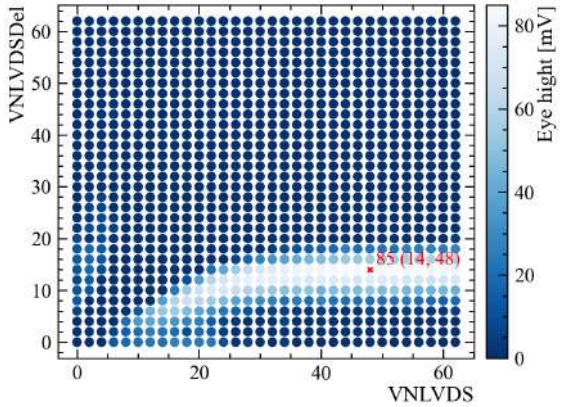

(c) Scatter Plot - eye height

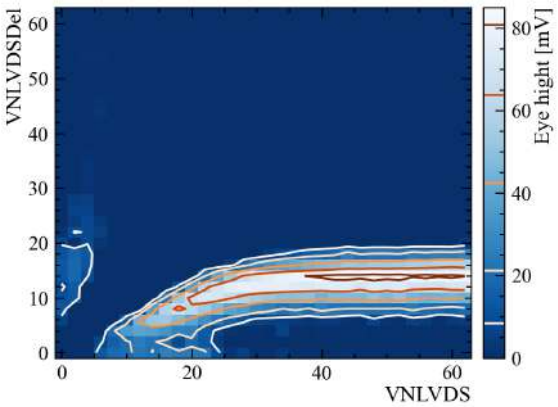

(d) Contour Plot - eye height

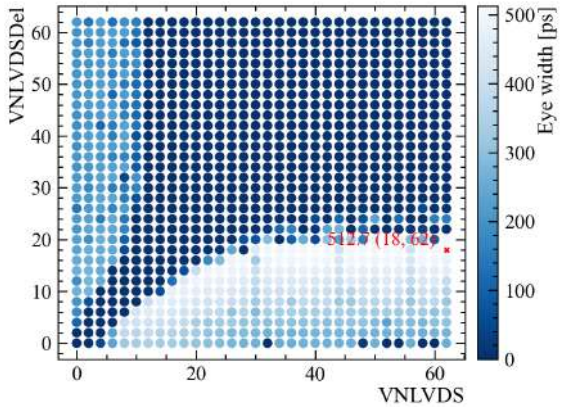

(e) Scatter Plot - eye width

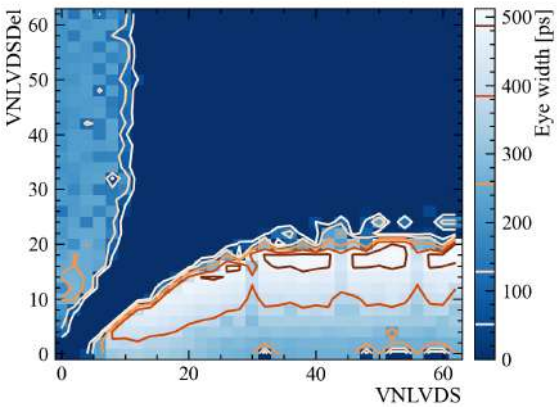

(f) Contour Plot - eye width

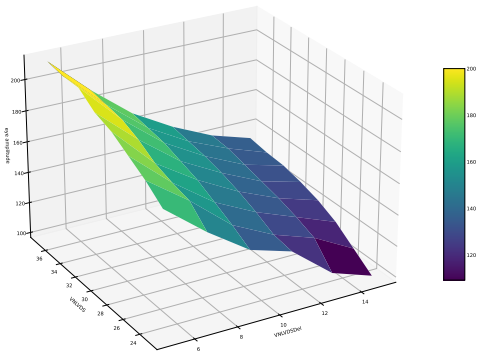

(g) 0463-00003-000001 - amplitude

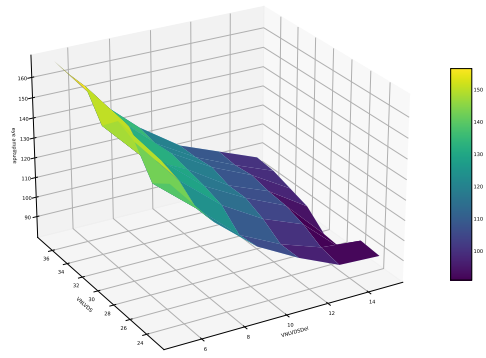

(h) 0463-00003-000002 - amplitude

6.2 Measurement of VNDcl and VPDcl

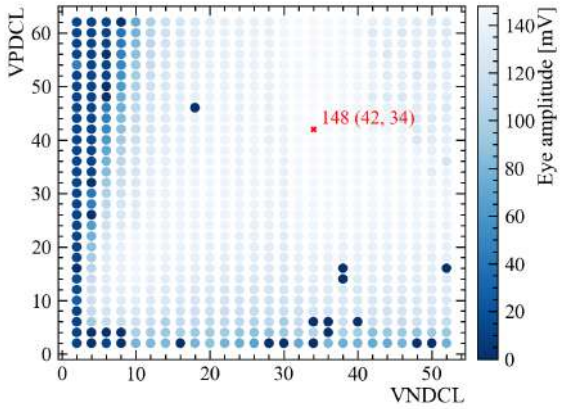

(i) Scatter Plot - eye amplitude

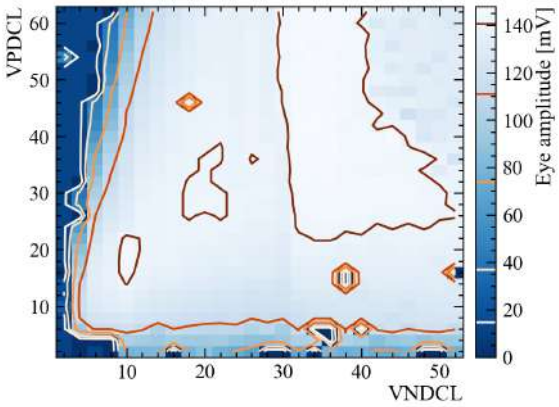

(j) Contour Plot - eye amplitude

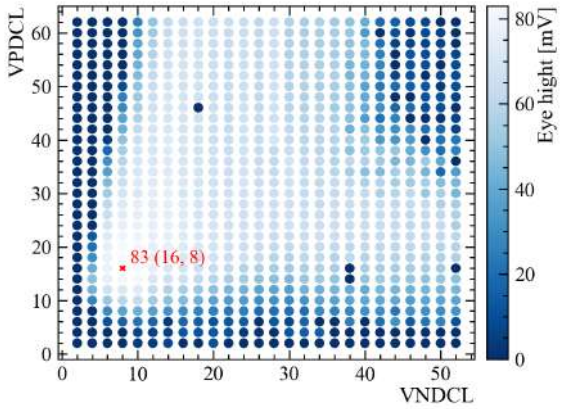

(k) Scatter Plot - eye height

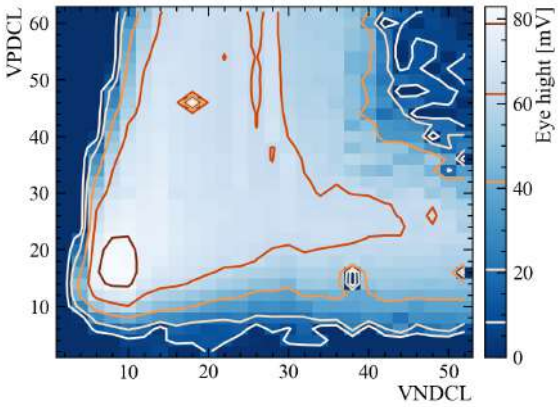

(l) Contour Plot - eye height

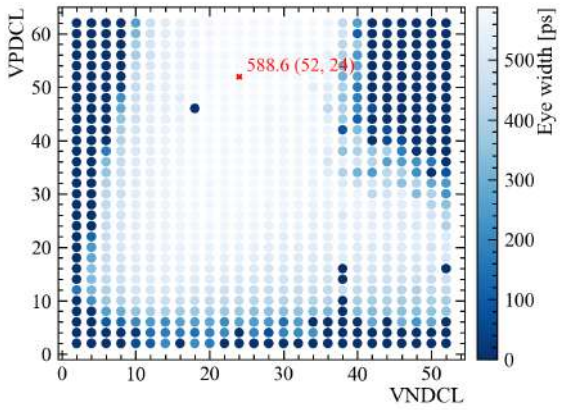

(m) Scatter Plot - eye width

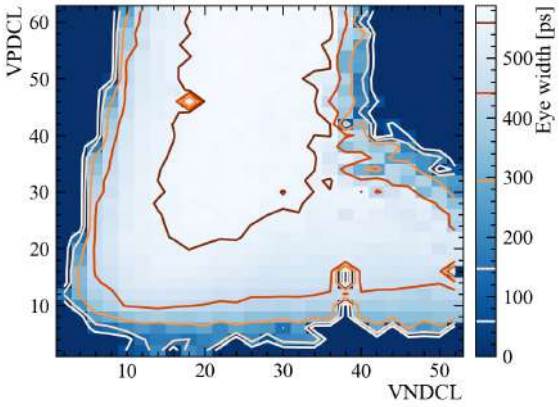

(n) Contour Plot - eye width

6.3 List of Acronyms

PSI Paul Scherrer Institute . . . 1
SDA Serial Data Analyzer . . . 1
HV-MAPS High-Voltage Monolithic active pixel sensor . . . 1
VNA Vector Network Analyzer . . . 1
DAQ Data Acquisition System . . . 1
BER Bit Error Rate . . . 1
SciTile Scintillating Tile . . . 1
SciFi Scintilating Fibre . . . 1
QC Quality Control . . . 2
DAC Digital to Analog Converter . . . 3
QCD Quantum Chromodynamics . . . 3
HiMB High-Intensity Muon Beamline . . . 8
CMOS Commercial Metal-Oxide-Semiconductor . . . 14
ToF Time of flight . . . 14
CSA Charge sensitive amplifier . . . 15
ToT Time over Threshold . . . 16
TDAC Tuning/Trimming Digital to Analog Converter . . . 17
HDI High-Density Interconnect . . . 17
SpTAB Single-point Tape- Automated Bonding . . . 17
MuTRiG Muon Timing Resolver including Gigabit-link . . . 19
FEB Front-end board . . . 21
DAB Detector Adapter Board . . . 21
CMS Compact Muon Solenoid . . . 22
DAB-STP Detector adapter board - shielded twisted pair . . . 23
BoSSL Adapter Board for Signal, Slow control and Low & high voltage for the vertex detector . . . 23
SMB-utp SubMiniature B - micro-twisted pair . . . 23
DC Direct Current . . . 25
AC Alternating Current . . . 25
NEXT Near End Crosstalk . . . 26
FEXT Far End Crosstalk . . . 26
PLL Phase-Locked Loop . . . 30
FPGA Field Programmable Gate Array . . . 58
GPU Graphics Processing Unit . . . 59
MIDAS Maximum Integration Data Acquisition System . . . 59
Dcl Differential current line . . . 63
VCO Voltage-controlled oscillator . . . 63
LVDS Low-Voltage Differential Signaling . . . 63

Bibliography

[1] *Das Paul Scherrer Institut in Kürze — psi.ch.* https://www.psi.ch/de/about/das-psi-in-kuerze. [Accessed 14-12-2023].

[2] W. N. Cottingham and D. A. Greenwood. *An Introduction to the Standard Model of Particle Physics*. 2nd ed. Cambridge University Press, 2007. DOI: 10.1017/CBO9780511791406.

[3] Wikipedia. *Standard Model*. Wikimedia Foundation. Wikimedia Foundation. 2023. URL: https://en.wikipedia.org/wiki/Standard_Model.

[4] Y. Fukuda and et al. "Evidence for Oscillation of Atmospheric Neutrinos". In: *Phys. Rev. Lett.* 81.8 (Aug. 1998), pp. 1562–1567. ISSN: 1079-7114. DOI: 10.1103/PhysRevLett.81.1562. arXiv: hep-ex/9807003.

[5] Klaus Jungmann. "Aspects of Fundamental Muon Physics". In: (Sept. 1999).

[6] Yoshitaka Kuno and Yasuhiro Okada. "Muon Decay and Physics beyond the Standard Model". In: *Rev. Mod. Phys.* 73.1 (Jan. 2001), pp. 151–202. ISSN: 1539-0756. DOI: 10.1103/RevModPhys.73.151. arXiv: hep-ph/9909265.

[7] G. Hernández-Tomé, G. López Castro, and P. Roig. "Flavor Violating Leptonic Decays of τ and μ Leptons in the Standard Model with Massive Neutrinos". In: *The European Physical Journal C* 79 (Jan. 2019), p. 84. ISSN: 1434-6052. DOI: 10.1140/epjc/s10052-019-6563-4. arXiv: 1807.06050.

[8] A. Blondel et al. *Research Proposal for an Experiment to Search for the Decay $\mu- > eee$*. 2013. arXiv: 1301.6113 [physics.ins-det].

[9] Ralph Eichler and Christoph Grab. "The SINDRUM-I Experiment". In: *SciPost Phys. Proc.* (2021), p. 007. DOI: 10.21468/SciPostPhysProc.5.007. URL: https://scipost.org/10.21468/SciPostPhysProc.5.007.

[10] *A two-part upgrade for the proton accelerator — psi.ch.* https://www.psi.ch/en/media/our-research/a-two-part-upgrade-for-the-proton-accelerator. [Accessed 27-12-2023].

[11] Meroli Stefano. *Exploring the Physics of Multiple Scattering for Particles in Matter — meroli.web.cern.ch.* https://meroli.web.cern.ch/lecture_multiple_scattering.html. [Accessed 27-12-2023].

[12] Timothy Carlisle. *Multiple Scattering (MSC) in Geant4*. https://indico.cern.ch/event/190654/contributions/345614/attachments/270741/378860/CM33_ScatteringOverview.pdf. [Accessed 27-12-2023].
[13] K. Arndt et al. "Technical design of the phase I Mu3e experiment". In: *Nuclear Instruments and Methods in Physics Research Section A: Accelerators, Spectrometers, Detectors and Associated Equipment* 1014 (2021), p. 165679. ISSN: 0168-9002. DOI: https://doi.org/10.1016/j.nima.2021.165679. URL: https://www.sciencedirect.com/science/article/pii/S0168900221006641.
[14] A. Bravar et al. *Development of the Scintillating Fiber Timing Detector for the Mu3e Experiment*. 2022. arXiv: 2208.09906 [physics.ins-det].
[15] Ivan Perić et al. "High-voltage CMOS active pixel sensor". In: *IEEE Journal of Solid-State Circuits* 56.8 (2021), pp. 2488–2502.
[16] Meroli Stefano. URL: https://meroli.web.cern.ch/lecture_hybrid_pixel_detector.html.
[17] Renato Turchetta. "CMOS monolithic active pixel sensors (MAPS) for scientific applications". In: (2003).
[18] J. Hammerich. "Towards MightyPix, an HV-MAPS for the LHCb Mighty Tracker upgrade". In: *Journal of Instrumentation* 17.10 (Oct. 2022), p. C10005. DOI: https://doi.org/10.1088/1748-0221/17/10/c10005.
[19] Heiko Augustin et al. "The MuPix sensor for the Mu3e experiment". In: *Nuclear Instruments and Methods in Physics Research Section A: Accelerators, Spectrometers, Detectors and Associated Equipment* 979 (2020), p. 164441. ISSN: 0168-9002. DOI: https://doi.org/10.1016/j.nima.2020.164441. URL: https://www.sciencedirect.com/science/article/pii/S016890022030838X.
[20] I Perić A Weber and H Augustin. *Mupix10 Documentation*. Tech. rep. Technical Report, μ 3 e Internal Note 52, 2020, Version 0.6.
[21] Hermann Kolanoski and Norbert Wermes. *Teilchendetektoren*. Springer, 2008.
[22] URL: https://indico.physi.uni-heidelberg.de/event/439/contributions/1244/attachments/640/847/MuPix11_Submission_Review_SIides.pdf.
[23] Thomas Rudzki et al. "The Mu3e experiment: Toward the construction of an HV-MAPS vertex detector". In: *arXiv preprint arXiv:2106.03534* (2021).
[24] Huangshan Chen and et al. "Characterization Measurement Results of MuTRiG - A Silicon Photomultiplier Readout ASIC with High Timing Precision and High Event Rate Capability". In: *PoS TWEPP-17*. 2017, p. 008. DOI: 10.22323/1.313.0008.
[25] Mu3e. *Mu3e Micro-twisted pai connections*. Internal Note. 2023.
[26] Mu3e. *Instructions to operate rope machine for bundling microtwisted pair cables*. Internal Note. 2023.
[27] Frank Meier. *The Mu3e ultra-low-mass tracker*. https://indico.cern.ch/event/695767/contributions/3014935/attachments/1674108/2686948/praesMu3eValencia2018.pdf. [Accessed 20-12-2023].
[28] Beat Meier. *Readout Cables Inside Detector Mu3e Integration Meeting*. https://indico.psi.ch/event/6594/contributions/13931/attachments/

12006/15381/20180619_Mu3e_Meeting_Beat_Meier.pdf. [Accessed 20-12-2023]. 2018.
[29] Mu3e. *Microtwisted pair cable order form*. Order form. 2023.
[30] R. B. Darling and W. Sun. 2013. URL: https://people.ece.uw.edu/darling/AgilentRFLab/Transmission%20Lines%20and%20Reflected%20Signals.pdf.
[31] URL: https://www.elektronik-kompendium.de/sites/grd/0301035.htm.
[32] URL: http://openelectrical.org/index.php?title=Cable_Sizing_Calculation.
[33] R.W. Beatty. "Insertion loss concepts". In: *Proceedings of the IEEE* 52.6 (1964), pp. 663–671. DOI: 10.1109/PROC.1964.3047.
[34] Smt. *What is insertion loss? what is return loss?* May 2020. URL: https://somanytech.com/what-is-insertion-loss-what-is-return-loss/.
[35] May 2020. URL: https://www.flukenetworks.com/knowledge-base/dtx-cableanalyzer/attenuation-insertion-loss-measurement-and-testing-dtx.
[36] URL: https://www.polarinstruments.com/support/si/AP8196.html.
[37] Alexandru Spătaru. *Theorie der Informationsübertragung*. Berlin, Boston: De Gruyter, 1973. ISBN: 9783112550823. DOI: doi:10.1515/9783112550823. URL: https://doi.org/10.1515/9783112550823.
[38] URL: https://cds.cern.ch/record/483309/files/p572.pdf.
[39] Mar. 2022. URL: https://www.flukenetworks.com/blog/cabling-chronicles/cable-testing-101-cross-talk-near-and-far.
[40] Gary Breed. "Bit Error Rate: Fundamental Concepts and Measurement Issues". In: *High Frequency Electronics* (Jan. 2003), pp. 46–48. DOI: https://www.highfrequencyelectronics.com/Jan03/HFE0103_Tutorial.pdf.
[41] Download PDF. *An introduction to preemphasis and equalization in maxim GMSL Serdes devices*. Aug. 2023. URL: https://www.analog.com/en/technical-articles/an-introduction-to-preemphasis-and-equalization-in-maxim-gmsl-serdes-devices.html.
[42] URL: https://scdn.rohde-schwarz.com/ur/pws/dl_downloads/dl_common_library/dl_brochures_and_datasheets/pdf_1/ZNB_dat-sw_en_3608-3278-22_v0600.pdf.
[43] *web.mit.edu*. https://web.mit.edu/6.013_book/www/chapter14/14.6.html. [Accessed 21-12-2023].
[44] Nov. 2022. URL: https://blog.teledynelecroy.com/2022/11/sdaiii-and-qualiphy-software.html.
[45] J FLEIG and J MAIER. In: *Journal of Electroceramics* 1.1 (1997), pp. 73–89. DOI: 10.1023/a:1009902532596.
[46] URL: https://control.com/textbook/ac-electricity/transmission-lines/.
[47] *minicircuits.com*. https://www.minicircuits.com/pdfs/TCM2-33X+.pdf. [Accessed 18-12-2023].
[48] URL: https://www.eecs.yorku.ca/course_archive/2011-12/F/3213/Notes/chapter_3.pdf.

[49] URL: https://www.allaboutcircuits.com/tools/twisted-pair-impedance-calculator/.

[50] Marius Köppel. "Data Flow in the Mu3e DAQ". In: *IEEE Transactions on Nuclear Science* 70.6 (June 2023), pp. 898–905. ISSN: 1558-1578. DOI: 10.1109/tns.2023.3276470. URL: http://dx.doi.org/10.1109/TNS.2023.3276470.

[51] David Maximilian Immig. URL: https://www.physi.uni-heidelberg.de/~immig/report/masterthesis_immig.pdf.